# Chapter 5

## Synthesis of $Fe_3O_4$ Nanoparticles using *edta* as Template, Their characterization and Applications as Vectors for Drug Delivery and MRI Contrast Agent

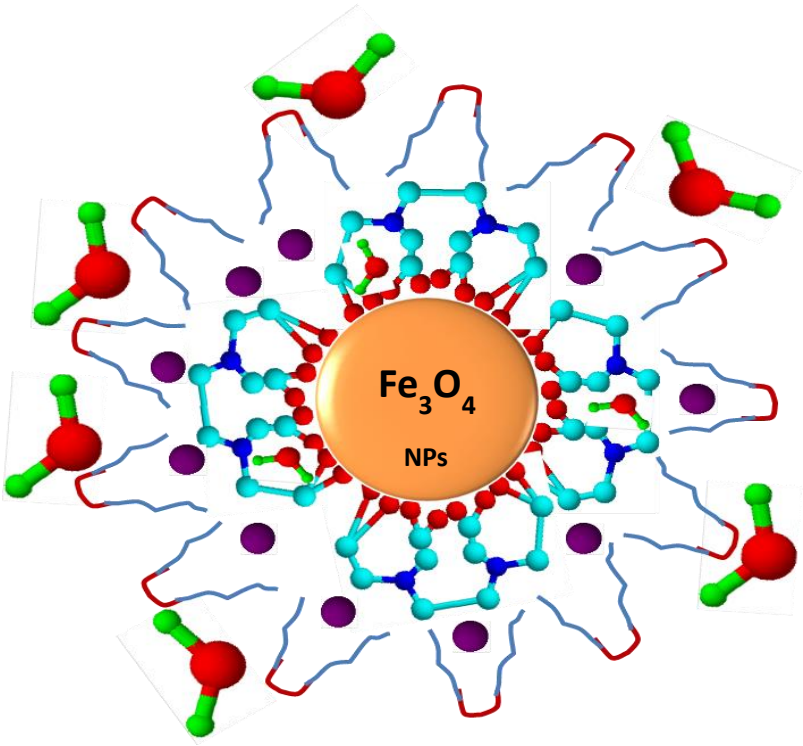


**EDTA Capped Iron Oxide Nanoparticles Magnetic Micelles: Drug Delivery Vehicle for Treatment of Chronic Myeloid Leukemia and $T_1$-$T_2$ Dual Contrast Agent for Magnetic Resonance Imaging**

*This study shows that multiple functionalities like drug delivery and $T_1$-$T_2$ dual modalities can be achieved by proper surface architecturing!*

*Revision Submitted in*

*R.Sc*

**New Journal of Chemistry**

## 5.1 Introduction

Nowadays, nanoscience and nanotechnology are boon to the patients suffering from diseases like cancer, diabetes, alzimers etc. Especially in the case of cancer, it requires early and explicit diagnosis followed by target specific treatment. [1, 2]The traditional treatment like chemotherapy is vigorous and non-specific. Ideally, factors like psychology of the patients, efficacy of the drugs for the disease, immune response, competence of the patient toward drug dosages etc should be considered before adopting any treatment for cancer. Established drugs (like cis-platin, taxol, paclitaxol etc) available in the market even though highly effective causes many side-effects in patient due to non-specificity and insolubility in body fluid. [3, 4]Many strategies have been developed for the purpose. For example, the drug is entrapped in micro or nanocavity of carrier like cyclodextrin or micelles having hydrophilic/hydrophobic surface. [5-8] However, this suffers from the disadvantage of enzymatic degradation of vehicle on its way into target cells. Further, even if the vehicle with the loaded drug reaches the target cells, cell transfection remains a major issue.[9, 10]

Surface engineered Super Paramagnetic Iron Oxide Nanoparticles (SPIONs) are the best option available for the purpose. The possible areas of applications of

SPIONs are highlight in Figure 5.1. The advantages of SPIONs as drug carrier over the traditional delivery vehicles are [11, 12]: (1) the particle size, shape and surface charge can be tuned according to requirement. It was observed that particles having size larger than 200 nm are removed from the body by liver, spleen and reticuloendothelial system (RES) while those of less than 5 nm are rapidly excreted through the kidney. [13]

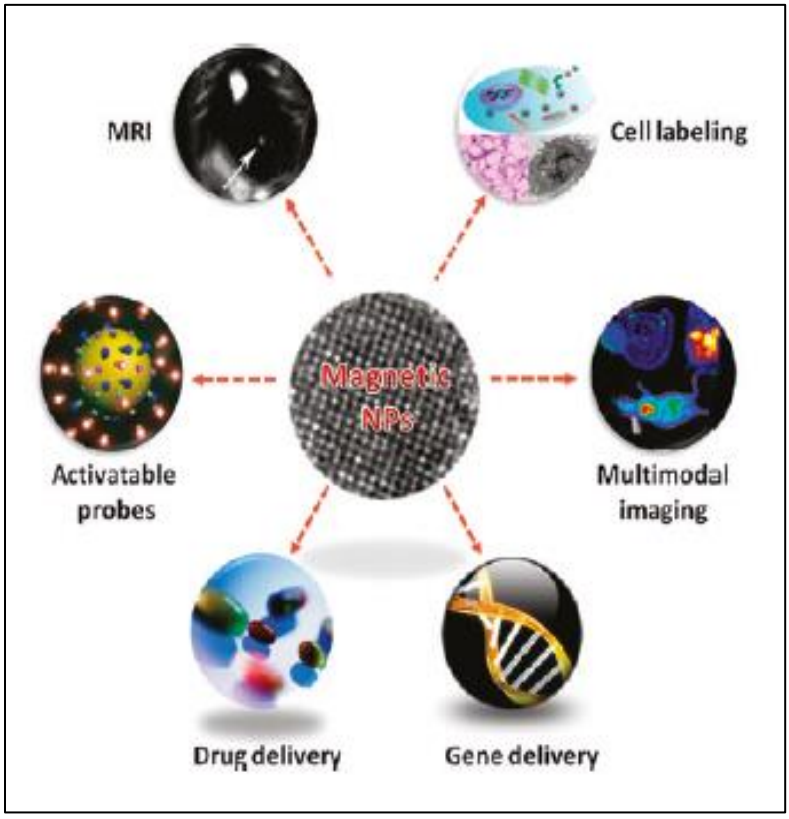


**Figure 5.1**. The fields where the iron oxide nanoparticles find application (J Xie,G Liu,H S. Eden,H Ai, X Chen,*Acc. Chem. Res*., 2011, **883**,44).

However, the circulation life time of the particles (having definite size) in the blood can be extended and tuned by varying the nature (hydrophilic/hydrophobic) of coating materials around the core. Various functionalities (drug, plasmids, small organic molecules, antibody etc, Figure 5.2) can be anchored on to the surface of nanoparticles by adjusting the surface charge which in turn, depends on presence of excess anions or cations in the surrounding.

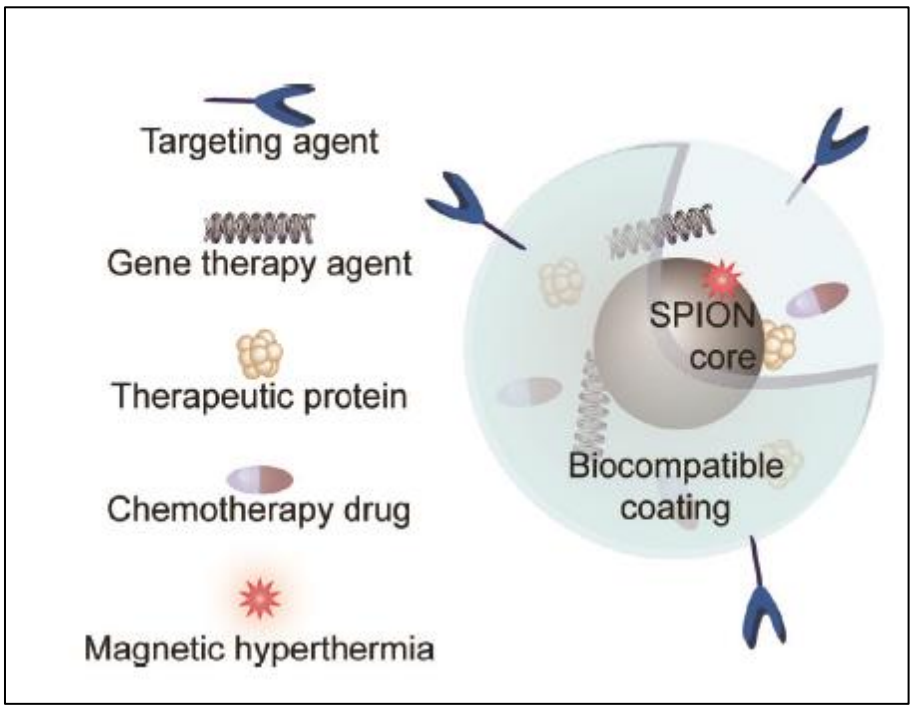


**Figure 5.2.** Various functionalities can be attached on the surface of $Fe_3O_4$ Nanoparticles (F. M. Kievit, M. Zhang, *Acc. Chem. Res*.,2011, **853**,10).

(2) The behavior of the material in response to applied magnetic field can be tuned with the particle size. It is known that the magnetic material contains magnetic domains having randomly oriented magnetic moments in the absence of applied

magnetic field. When particle size decreases to about 20 nm, these domains merges into a single domain having one collective magnetization direction in the applied field (Figure 5.3).[14, 15] Due to this, magnetic NPs have a natural tendency to agglomerate and increase their size and in turn, reduce their blood circulation time which is not desired.[16] For this reason, super paramagnetic NPs are preferred which can become magnetized only on exposure to applied field and can get immediately demagnetized on removal of the field. Therefore, SPIONs should have zero coercivity with no hysteresis. These make SPIONs a unique tool in MR imaging as contrast agent of type $T_2$ (darken the lesions with respect to surrounding environment). [17-19]

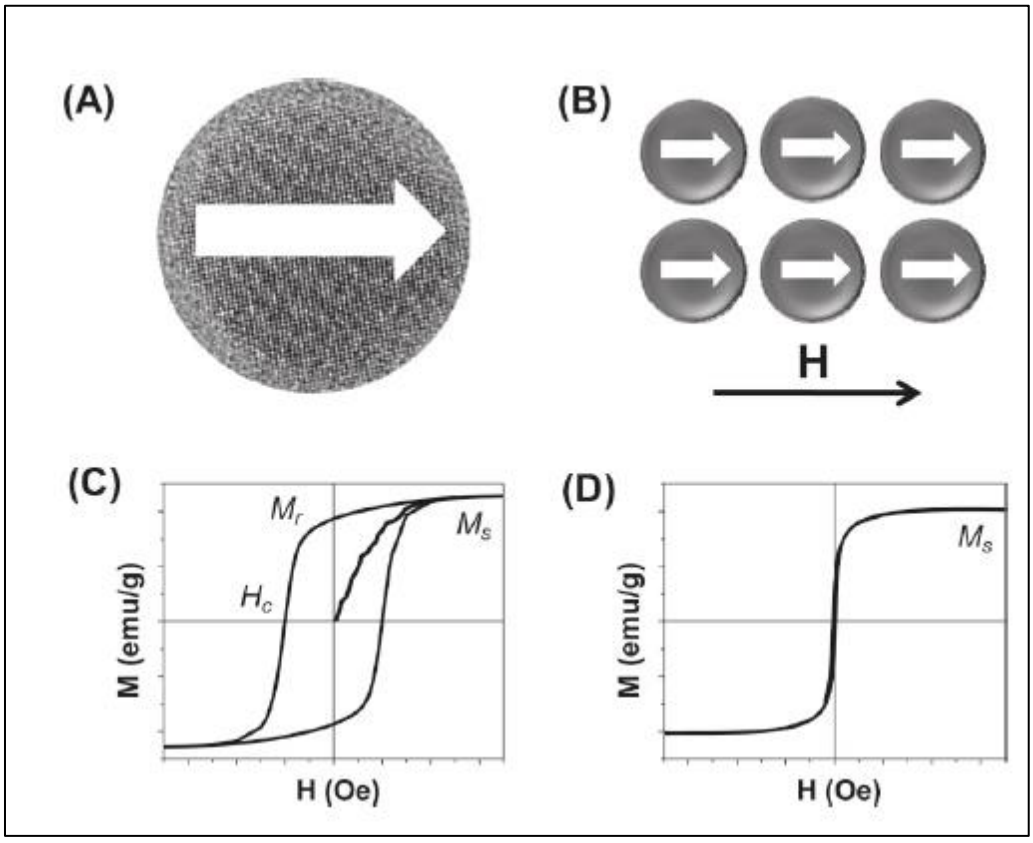

**Figure 5.3**. (A) a single domain magnetic NP with its magnetization pointing to one direction, (B) a group of single domain magnetic NPs aligned along a magnetic field direction, (C) the hysteresis loop of a group of ferromagnetic NPs, and (D) the hysteresis loop of a group of superparamagnetic NPs (D Ho, X Sun, S Sun, Acc. Chem. Res,2011, **875**,44).

The efficiency of the contrast agent (as $T_1$ or $T_2$) depends on its particle size, surface charge, presence of coordinated water, strength of applied magnetic field as well as local magnetic field produced due to paramagnetic nature of the material in response to applied field etc. [20]In an ideal case, contrasting efficiency can be compared with twinkling of the stars in the background of the night sky. Same way, contrasting agent should enhance (or nullify) the signals coming from lesions compared to other regions. Generally, commercially available Gd or Mn based chelates (eg. Gd-DTPA or Magnevist®) which act as $T_1$-constrast agents consist of cyclic DOTA ligand (1,4,7,10-tetraazacyclododecane-1,4,7,10-tetraacetic acid) or its acyclic analogue DTPA (diethylenetriaminepentacetic acid) possessing 8-donar atoms while, the ninth coordination valence of Gd ions is satisfied by water molecule (Figure 5.4). [21-23] Such type of water molecules known as inner sphere water molecules are mainly responsible for contrasting effect due to different longitudinal relaxation rate than normal 'bulk' water molecules present in the vicinity. [24]

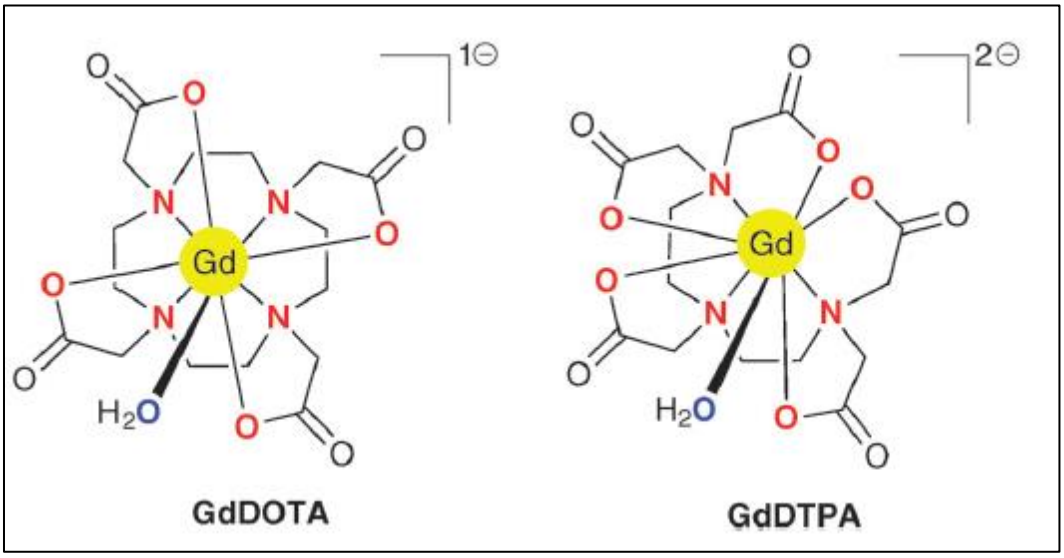


**Figure 5.4.Chemical structures of GdDOTA and GdDTPA.**

On the contrary, SPIONs direct the transverse relaxation ($T_2$) of protons and generate the dark signal enhancement (Figure 5.5). Traditional MR imaging using $T_1$ or $T_2$ contrast agents has certain limitations related to refinement of signals originating from artifacts (such as fat, calcification, hemorrhages, air etc) other than diseased lesions. [25] These make the image complicated and difficult to map the area of disease spread, in most cases.

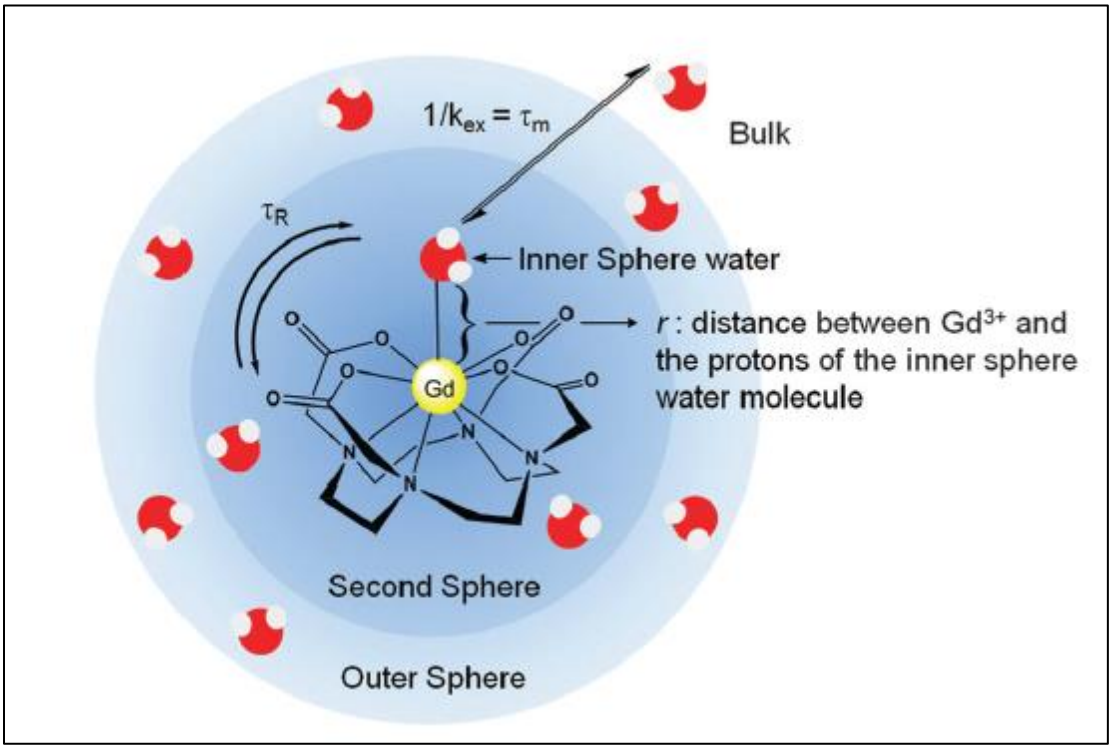


Figure 5.5.A graphical representation of the factors influencing a contrast agent's relaxivity (P.Verwilst, S. Park, B. Yoon and J. S. Kim, *Chem. Soc. Rev.*, 2015,**1791**,44).

One of the solutions of this problem is to design $T_1$-$T_2$ dual mode contrast agent i.e. insertion of $T_1$ contrast agent to the matrix of $T_2$ agent. Bae et al developed conjugated $T_1$-$T_2$ dual mode contrast agent by covalent attachment of Gd-chelate based $T_1$ contrast agent to dopamine covered iron oxide NPs through isothiourea linkage. For this modality developed by them, the obtained $r_1$ value 11.7 and $r_2$ value 30.32 $mM^{-1}s^{-1}$ make it capable to act as $T_1$-$T_2$ dual mode contrast agent (Figure 5.6). [26]

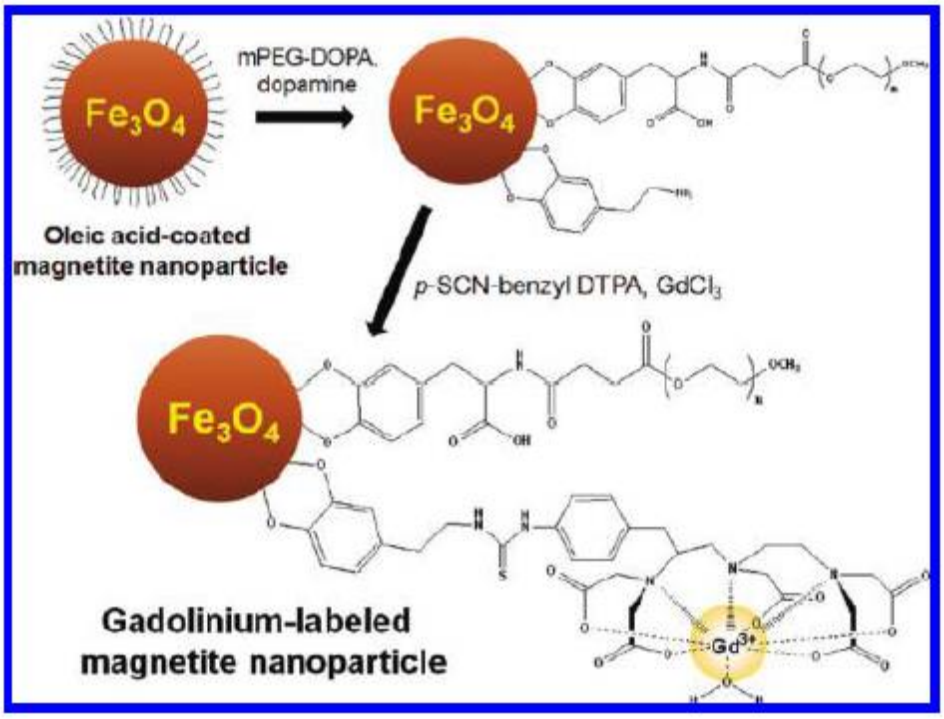


**Figure 5.6. Synthesis of gadolinium-labeled magnetite nanoparticles (GMNPs) as dual contrast agents for *T*1- and*T*2-weighted magnetic resonance imaging** (K. H. Bae, Y. B. Kim, Y. Lee, J. H. Wang, H. Park and T.G. Park, *Bioconjugate Chem.*,2010, **505**, 21).

Attempts have also been made to dope $T_1$ contrast agent ($Gd_2O_3$ or Mn) in the matrix of $T_2$ contrast agent (iron oxide) which improved the quality of MR imaging of hepatic tumor in mice. [27, 28] However, the leaching of dopant metal ions (particularly Gd) from the host matrix was a major safety issue to be solved. It was observed that these leached Gd ions, upon organ uptake, cause toxic side effects such as nephrogenic systemic fibrosis (NSF). [29, 31]Therefore, it is desirable to develop a contrast agent, either single or dual mode free from Gd ions. Considering these points, we can design the structure of the contrasting agent such that both $T_1$

and $T_2$ modalities can be induced in a single material. For example, $r_2$ relaxivity can be achieved by controlling the particle size of the SPIONs and $r_1$ by mimicking the working mechanism of Gd complexes.

Chronic Myeloid Leukemia (CML) is a form of cancer of bone marrow due to increased and unregulated growth of myeloid cells and resulting accumulation in the blood. This occurs due to -translocation of Philadelphia chromosome- a genetic abnormality.[32] CML accounts for approx. 20% of adult leukemia and annual incidences ranges from 0.8-2.2 in male and 0.6-1.6 in female per one lac population in India. [33]

The fact that Tyrosine Kinase Inhibitor (TKI) targets (inhibits) the BCR-ABL protein, responsible for activation of cascade of proteins that control the cell cycle and speed up the cell division, proves its usefulness in the treatment of the disease.[34]Imatinibmesylate (signal transduction inhibitor STI-571) is one of the drugs of TKI class. [35] However, the treatment exerts many side-effects like nausea, muscle cramps, rash, abdominal pain, immune suppression and the worst is left ventricular dysfunction with severe congestive heart failure. [36 -38]These short-comings need to be tackled for better management of the treatment. Most of these adverse and toxic effects were formed due to the distribution of drug throughout the body. If imatinib is targeted directly to the diseased sites (bone marrow, in this

case) maximum response with minimum side effects can be achieved. SPIONs can do this function very well based on the strategy that they can last longer at the target site with controlled release of predecided dosage of the drug together with monitoring the progress in disease abatement. The logic of selecting $Fe_3O_4$ as vehicle to load imatinib and targeting bone marrow is as follows: Hemoglobin synthesis occurs in the developing red blood cells in the bone marrow, a process called erythropoiesis. As iron is the main constituent of hemoglobin, huge amount of iron is utilized during this process. Oral iron has the advantage of being simple and cheap, but it is limited by side-effects, poor compliance, poor absorption and low efficacy. Intravenous delivery of iron to the bone marrow is the best option available.[39] Iron makes complex with the transferrin protein present in the plasma. The transferrin receptors located on the surface of bone marrow cell line easily recognized this iron-protein complex and allows entering the same to the cell. On delivering drug to the bone marrow, iron oxide NPs would get accumulate naturally in the bone marrow as a precursor of hemoglobin to take part in erythropoiesis. Hence, SPIONs can be simultaneously used as vehicles for controlled drug delivery (therapeutic) and as MRI contrast agents (diagnostics). This makes them 'theranostic' agents in a true sense.

In the present work, we have reported the synthesis of iron oxide nanaoparticles using *edta* as capping agent. Pluronic-F127, a surfactant triblock co-polymer was

used to encapsulate the *edta*/$Fe_3O_4$ NPs. The resulting magnetic micelle having *edta* capped $Fe_3O_4$ NPs as core and pluronic as shell was transfected into human bone marrow K562 cell-line *in vitro* to evaluate cell death. In vivo MR imaging of bone marrow was performed on female albino wistar rat in presence and absence of magnetic field. It was observed that the synthesized magnetic micelles ($Fe_3O_4$/*edta*/pluronic) act as $T_1$-$T_2$ dual contrast agent. The probable mechanism for showing the dual mode contrasting effect is also discussed.

## 5.2 Experimental

### 5.2.1 Materials

Ferric Chloride $FeCl_3.6H_2O$was obtained from Loba chemicals, India. Ferrous Chloride $FeCl_2.2H_2O$, Ethylene diamminetetraacetate (*edta*) and sodium hydroxide (NaOH) were purchased from S D Fine Chemicals, India. Pluronic F-127 was purchased from Sigma Aldrich. All chemicals were AR grade and used without further purification.

### 5.2.2 Synthesis of $Fe_3O_4$/*edta* NPs

$Fe_3O_4$ NPs were synthesized by simple co-precipitation method. Aqueous solution of hydrochloric acid (400µL of 0.32M HCl) was added dropwise to the mixture of 50 mL aqueous solution of $FeCl_3$ .$6H_2O$ (0.24 mmol) and $FeCl_2.2H_2O$ (0.121 mmol) and stirred vigorously under the flow of nitrogen. To this solution, 25 mL

of aqueous solution of *edta* (0.24 mmol) together with 25 mL 1M NaOH solution were introduced. Then, temperature of reaction mixture was gradually raised to 70 $^{o}$C. The reaction mixture was further stirred under $N_2$ atmosphere for about 1 h to obtain a homogenous mixture. The reaction mixture was then centrifuged at 8000 rpm for 5 min and subsequently washed three times with water and ethanol to remove unreacted impurities and dried at 60 $^{o}$C under vacuum for two days.

### 5.2.3 Synthesis of imatinib loaded $Fe_3O_4$/*edta*/P magnetic micelles

300 mg of $Fe_3O_4$ nanoparticles were dispersed in 30 mL of milliQ water and then 100 mg of Pluronic F-127 was added. The mixture was then stirred overnight on magnetic stirrer at RT and then centrifuged at 6000 rpm for 5 min to get pluronic-F127 functionalized $Fe_3O_4$/*edta* NPs. 30 mg of these nanoparticles were dispersed in 10 mL of milliQ water. To it 2 mL of suspension containing drug solution (4.5 mg/mL) was added. Then the mixture was stirred vigorously on the magnetic stirrer at RT for about 24 h. The drug loaded $Fe_3O_4$ nanoparticles were allowed to settle down by a magnet. The magnet was kept outside the flask containing drug loaded nanoparticles for about 6 h and then the supernatant was decanted. The drug-loaded nanoparticles were suspended in milliQ water and washed twice.

The amount of drug loaded on nanoparticles was calculated by using UV-Visible spectroscopy. For that the drug solution varying in concentration from 0.5 to 9.0

mg/mL was prepared to construct calibration curve. It was found that every 1 mg of NPs, 0.12165 mg (121.65 µg) of drug was loaded.

Loading efficiency (%) = (Weight of drug loaded/ weight of total drug added) X 100

The loading efficiency was found to be 40.56 %

### 5.2.4 Characterization

X-ray powder diffraction (XRD) pattern of the $Fe_3O_4$/*edta* NPs was obtained from X-ray powder diffractometer (Bruker D8 Advance) with Cu Kα radiation, λ = 0.15418 nm. The mode of interaction of *edta* with the surface Fe ions of $Fe_3O_4$ NPs and the structure of magnetic micelles were studied using Fourier transform infrared spectroscopy (RX-FTIR, Perkin- Elmer, USA). The morphology of the samples was examined by Transmission Electron Microscopy (TEM, Philips Tecnai 20) at 200 kV. The hydrodynamic radius, size distribution and surface charge (in term of zeta potential, ζ) were measured using DLS technique at a scattering angle of $90^o$. A BIC 90 plus (Brookhaven) equipped with 35.0 mW solid state laser operating at 660 nm and an avalanche photodiode detector were used for the purpose. All measurements were made at 25 $^oC$ in deionized water. Differential Scanning Calorimetric (DSC) analysis and ThermoGravimetric Analysis (TGA) of $Fe_3O_4$/*edta* and $Fe_3O_4$/*edta*/P samples were carried out using Mettler Toledo DSC 822. For the purpose, the material was heated inside a DSC setup. The heating rate

was 10 $^{o}$C min$^{-1}$ from RT to 500$^{o}$C in $N_2$ atmosphere. The magnetic properties were studied on a vibrating sample magnetometer (VSM, Lakeshore 7410) at 298 K under an applied magnetic field of 15.000E+3 G.

A phantom study was carried out to determine the relationship between $T_1$ and $T_2$ relaxation times with various concentrations of $Fe_3O_4$/*edta*/P NPs. All the samples were prepared in aqueous medium. For phantom preparation, four samples having concentration of NPs (0.1, 0.05, 0.01, 0.001 mg mL$^{-1}$) were prepared and transferred into microcentrifuge tubes (2 mL). Pure water and *edta* solution (1 mg mL$^{-1}$) were taken as references. An array of microcentrifuge tubes was placed in a plastic container having water for magnetic field homogeneity. The phantom was carefully placed in the centre of the head coil, and MR imaging was performed at RT using clinical 1.5 T GE Medical Systems scanner in combination with 16-channel wrist joint coil. To determine $T_1$ relaxation time of each concentration, spin–echo (SE) sequences with different repetition times (TR; 60, 100, 200, 400, 600, 800, 1000, 2000, 3000, 5000 ms) and echo time (TE; 15 ms) were performed. The other imaging parameters were as follows: slice thickness = 7 mm, field of view (FOV) = 24 X 24 cm, matrix = 320 X 192, flip angle = 90$^{o}$ and imaging time = 1.0 min. For the measurement of $T_2$ relaxation time, SE protocol with following parameters was used: TR = 3000 ms with TE = 13, 24, 36, 99 ms, other parameters were same as described above.

Signal intensity in arbitrary units (a.u.) for each of the imaging sequences was obtained using Dicom (digital imaging and communication in medicine) Works software v 1.3.5 (Dicom Works, Lyon, France) via locating a circular region of interest (ROI) in the centre of each tube (maximum region of interest was considered). Recorded signal intensities were fitted in MATLAB (Mathworks, Natick, MA, USA) using the exponential eqn (1) and (2) to evaluate $R_1$ ($1/T_1$) and $R_2$ ($1/T_2$) relaxation rates, respectively.

$$Signal_{SE} = S_o(1 - e^{-TR/T1}) \quad (1)$$

$$Signal_{SE} = S_o(e^{-TE/T2}) \quad (2)$$

The slopes of $R_1$ and $R_2$ relaxations versus concentration of the samples were calculated as relaxivity values $r_1$ and $r_2$ in Origin 7.5.

### 5.2.5 *In vitro* cytotoxicity and cell culture study

K562 CML luekaemic cell line was cultured in Iscove's Dulbecco Eagle Medium and incubated at 37$^{o}$C in a humidified atmosphere containing 5% $CO_2$. After culturing sufficient amount of cells, the cell viability of $Fe_3O_4$/*edta*NPs and imatinib loaded magnetic NPs was carried out using trypan blue exclusion assay.

For the determination of the $IC_{50}$, $1x10^6$ cells were treated with serial concentrations of imatinib (0.125,0.25,0.5,1,1.5 µg/mL). For control, the same

amount of cells were added to the petri dish but without imatinib. The culture plates were then incubated for 24 hours at 37$^{o}$C in a humidified atmosphere containing 5% $CO_2$. The same experiment was carried out with drug loaded magnetic NPs micelles.

### 5.2.6 *In vitro* cytotoxicity test

Cytotoxicity of all the samples was tested on chronic myeloid leukemic cell line K562 by 3-(4,5-dimethylthiazol-2-yl)-2,5-diphenyltetrazolium bromide (MTT) assay (Sigma, USA). In complete full growth media K562 cells were seeded in a 96-well plate ($5\times10^3$ cells/well). Then, cells were treated with $Fe_3O_4$/*edta* NPs, imatinib mesylate loaded-NPs, and pristine imatinib mesylate of the same amount as loaded on NPs for 48 h at 37°C. After 48 h, the MTT was added to each well and the cells were incubated at 37° for 4 h. The medium was removed and dimethyl sulfoxide (DMSO) was added to dissolve the formazan crystals. The absorbance was measured at 570 nm with an ELISA reader. The experiments were performed in triplicate. The relative cell viability (RCV) w.r.t the control wells was calculated by the following equation: RCV = ($OD_{test}$ / $OD_{control}$) X 100%, where $OD_{test}$ and $OD_{control}$ were obtained in the presence and absence of the NPs, respectively.

### 5.2.7 *In vitro* drug release kinetics

To study drug release kinetics, three different experiments were performed. This study was carried out at 37 $^{o}$C and pH 7.4. In each experiment 3.0 mg of imatinib loaded magnetic NPs were added in flask having 30 mL $Na_2HPO_4$-$NaH_2PO_4$ buffer solution. The flask was then kept in shaker at 37$^{o}$C. The release medium was withdrawn at predetermined time intervals (1,2,3,4,5,6,7,8,9,12,24,36,48,60,80,100,124,148,172 and 196 h). The collected samples were analyzed using an uv-vis spectrophotometer (Perkin-Elmer Lambda 35) to determine the amount of imatinib released ($\lambda_{ex}$ 200 nm and $\lambda_{em}$301 nm).

### 5.2.8 *In vivo* studies

The animal protocol was approved by the Institutional Animal Care and Use Committee. *Wistar Rats* weighing 200 to 225 g were used after overnight fasting. Two groups of rats were employed for the study. Solution containing 2 mg imatinib in phosphate buffer pH 7.4 (equivalent to 100 mg/kg body weight) was administered intravenously through the tail vein to the first group while the second group was administered with $Fe_3O_4$/*edta*/P containing 2 mg drug by the same method.

Approximately, 0.1 mL of blood samples were collected from retro-orbital sinuses using heparinized capillaries into 1.5 mL micro-centrifuge tubes containing

heparin at 0 h predosage and then at every 1 h interval till 7 h post dose from each rat. At a predefined time interval after drug administration, animals were killed by stunning and blood was collected from carotid artery. After decapitation, both leg's femur and tibia bones were excised from the body and bone marrow was aspirated with the help of a needle. Similarly, livers were collected by dissection. Tissues were transferred to 20 mL glass tubes containing 1 mL of normal saline and homogenized at 10000 rpm for 1 min over ice. Samples were stored at -4°C till analysis. Plasma was separated by centrifugation at 4000 rpm for 7 min at 4°C. The plasma was then separated into 0.5 mL labeled micro-centrifuge tubes and stored at -4°C till analysis.

Tissue homogenates were made alkaline by adding 1 mL of 0.1 N NaOH and the drug was extracted by adding 2 mL ethyl acetate. The organic layer was separated after centrifugation at 5000 rpm for 15 min at $4^{o}$C and evaporated under vacuum. The residue was suspended in sodium heptane sulphonic acid in 0.01M $KH_2PO_4$ (pH 2.5) and methanol. Imatinib in all the tissue homogenates and plasma were estimated by HPLC method.

### 5.2.9 Histopathological analysis

All the steps for drug formulations, administration and animal killing were performed similar to above mentioned process. Blood, bone marrow, liver, spleen and kidney were collected by dissection and transferred to formalin immediately.

All the tissues and blood were then stabilized by attaching ultrathin sections on to a slide for permanent fixing.

### 5.2.10 Animal imaging

The MRI study was performed using clinical 1.5 T scanners to observe the accumulation of the iron oxide formulation in the bone marrow of Female Albino Wistar Rat. All the experiments were planned according to the guidelines of the animal ethical committee (IAEC/DPS/SU/1229 Dated 5th Sept. 2012). The rat bone marrow was observed as a standard (pre contrast) and bone marrow targeted action of the formulation was observed as post contrast MRI study. Before MRI, sedation of a rat was done with a mixture of ketamine and xylazine (2.3:1) where 1.66 μL per gram body weight was injected intraperitoneally. After sedation, imaging was done with a phase sensitive inversion recovery sequence, $T_1$-weighted images (with TE = 15 and TR = 1000) and $T_2$-weighted images (with TE = 99 and TR = 3000) were taken prior to, 15 min and 24 h post injection of micellar NPs (selected TE and TR values were as per optimized results of phantom study). Further parameters were set as: slice thickness (THK) = 1.44 mm; field of View (FOV) = 5 mm; matrix = 180×256×20) and was labelled as pre contrast imaging. After the standard imaging of the bone marrow, the micellar NPs formulation was injected intravenously in the body (400 μL 0.01 mg/mL NPs as per phantom study results) through the tail vein. The same sequence of imaging was performed after

15 min and then after 24 h of injection. The images were compared with the standard images of control.

## 5.2 Results and discussion

The general procedure for the synthesis of SPIONs NPs involves the co-precipitation of $Fe^{3+}$ and $Fe^{2+}$ salts to get $Fe_3O_4$ NPs in presence of *edta* ligands as capping agents. Here, *edta* was used based on the following strategy (1) it can act as a small molecular linker which can bind iron oxide nanoparticles with carboxylate groups and prevent them from agglomerating (2) increases the solubility of iron oxide nanoparticles in body fluid by chelating and bridging and also (3) the carboxylate groups chemisorb on to the surface of the nanoparticles making the inner sphere hydrophilic and the hydrocarbon part remains away from the surface making the outer sphere hydrophobic. Pluronic F127 ($EO_{102}PO_{78}EO_{102}$) is an amphiphilic triblock copolymer which can self-assemble into spherical micelle in aqueous medium in which poly (propylene oxide) chains form inner hydrophobic core while poly(ethylene oxide) chains form outer hydrophilic shell. [40] We had optimized the amount of pluronic required to encapsulate the $Fe_3O_4$/*edta* NPs surface completely. And accordingly, the concentration of pluronic was adjusted (20 mg/mL). [41] The resulting micellar assembly becomes capable to load hydrophobic drug imatinib.

### 5.3.1 Compositional, morphological and surface studies

The synthesized iron oxide nanoparticles were characterized by XRD to study crystallinity and phase of the material (Figure 5.7). The XRD patterns manifest predominant diffraction peaks at 2θ values 30.1, 35.15, 43.10, 53.50, 57.21 and 63.0 correspond to the (200), (311), (400), (422), (511), and (440) planes, respectively. These features indicate a magnetite phase with inverse spinel structure in which oxygen forms cubic face centered packed (FCC) arrangement and the Fe cations occupy the interstial *Td* and *Oh* sites. These standard peak positions indicate that coating of *edta* on $Fe_3O_4$ NPs as capping ligands does not affect the phase and crystallinity of the material. The particle size calculated from Debye-Schirrer formula ($L=0.9\lambda / \beta \cos\theta$) [42] and the FWHM (Full Width at Half Maximum) values corresponding to the major plane (311) was in the range of 56 nm. The compactness and clear resolution of the peaks indicate properly ordered and compact *edta* layer on the surface of NPs.

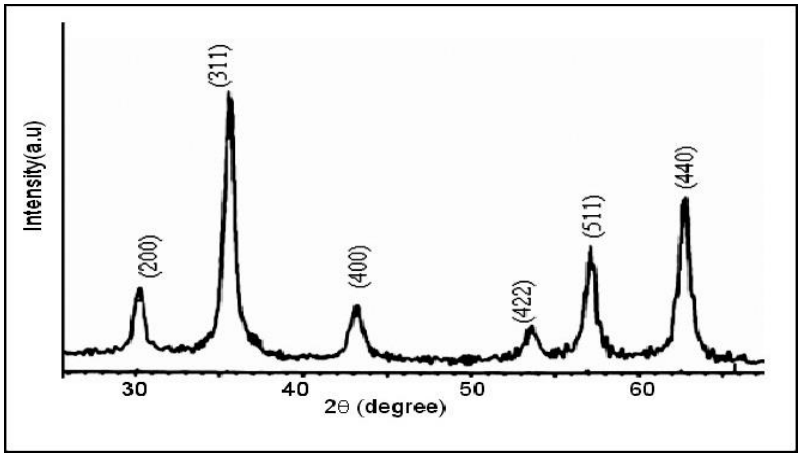


**Figure 5.7. XRD patterns of as-synthesized $Fe_3O_4$/*edta* nanoparticles.**

Further, the size and shape of $Fe_3O_4$/*edta* NPs were studied by TEM analysis. The TEM image shows spherical particles and size histogram shows that most of particles are present in the size range of 100-120 nm (Figure 5.2). Particle size was further measured by DLS technique (Figure 5.S1).

**Fe3O4 Aliquot (Combined)**

| | |
|---|---|
| **Effective Diameter:** | **252.5 nm** |
| **Polydispersity:** | **0.251** |
| **Avg. Count Rate:** | **1.4 Mcps** |
| **Baseline Index:** | **0.0** |
| **Elapsed Time:** | **00:02:30** |

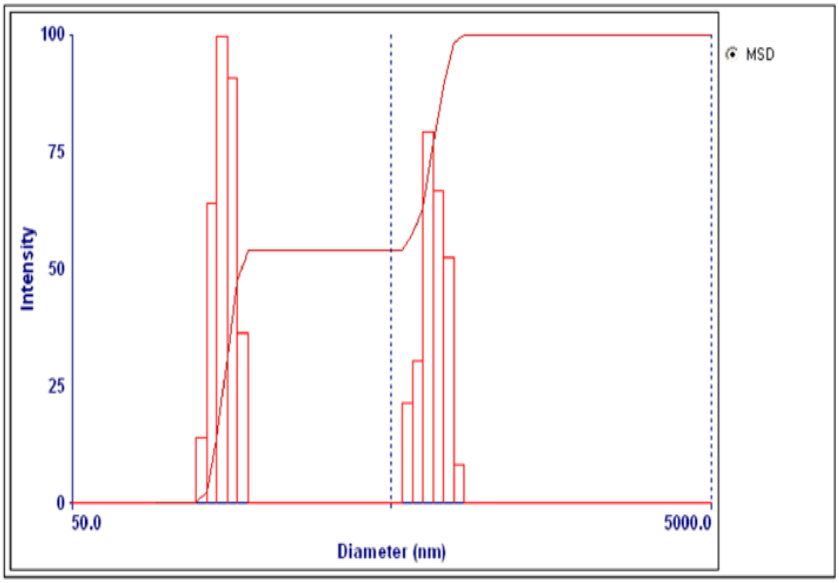


| Run | Eff. Diam. (nm) | Half Width (nm) | Polydispersity | Baseline Index |
|---|---|---|---|---|
| 1 | 247.5 | 50.8 | 0.042 | 0.0 |
| 2 | 232.8 | 126.1 | 0.294 | 0.0 |
| 3 | 226.1 | 117.5 | 0.270 | 0.0 |
| 4 | 312.0 | 178.8 | 0.328 | 0.0 |
| 5 | 551.7 | 296.1 | 0.288 | 0.0 |
| Mean | 314.0 | 153.9 | 0.245 | 0.0 |
| Std. Error | 61.3 | 41.0 | 0.051 | 0.0 |
| Combined | 252.5 | 126.4 | 0.251 | 0.0 |

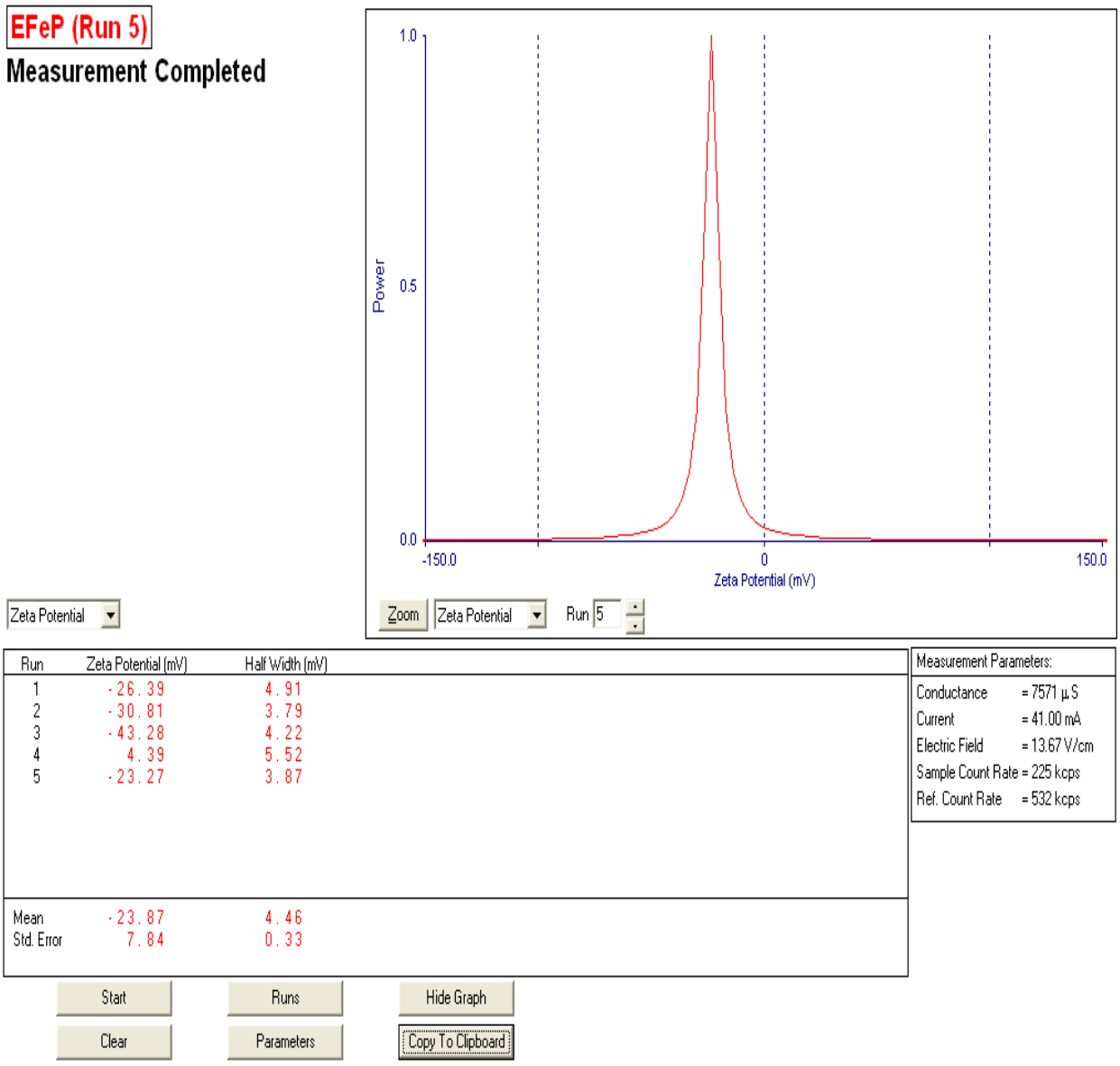


**Figure 5.S1. DLS and Zeta potential measurements of (a) $Fe_3O_4$/edta and (b) $Fe_3O_4$/edta/PNPs.**

The mean particle size for $Fe_3O_4$/*edta* NPs was 232 nm with a polydispersity index of 0.251. On addition of pluronic the average particle size increases to 440 nm with polydispersity index 0.005. The discrepancy in particle size measured by DLS and that of XRD and TEM was very well explained by Jain at al [43] DLS measures

overall hydrodynamic diameter of the NPs micelle resulting from hydration of $Fe_3O_4$/*edta* and $Fe_3O_4$/*edta*/P with aqueous media. The small value of polydispersity index for $Fe_3O_4$/*edta*/P system suggests ordered orientation of NPs assembly in aqueous media. In this study, *edta* plays a dual role; first it acts as a capping agent and restricts the growth of $Fe_3O_4$ crystal to the nano regime, secondly, it increases the dissociation rate of $Fe_3O_4$ NPs, mineralize it completely and merge the same into the blood pool. By this way it can reduce the toxicity of the material.

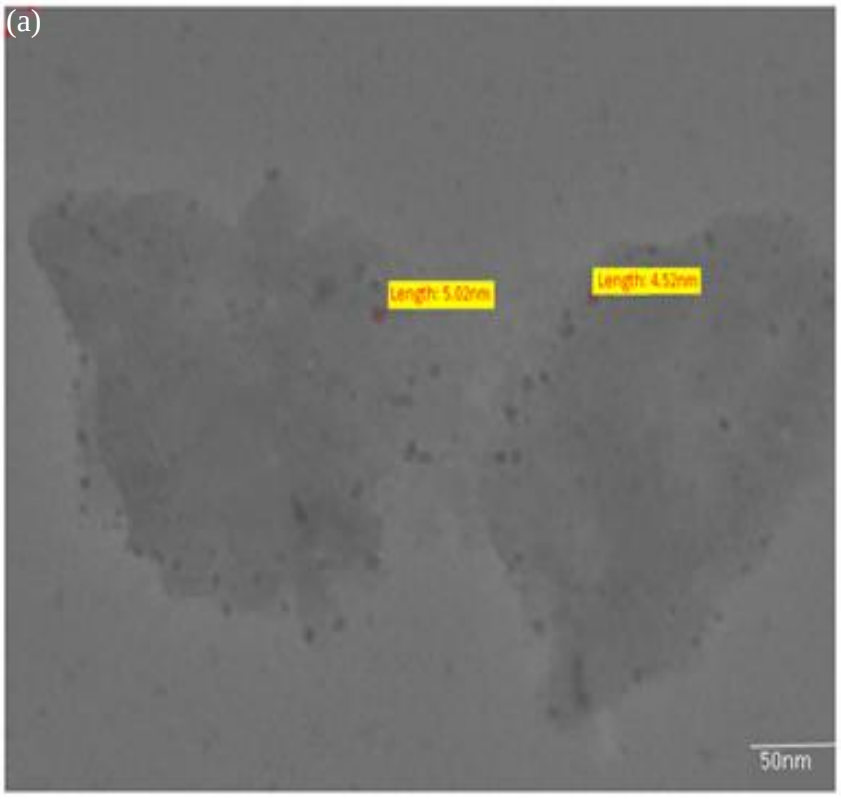

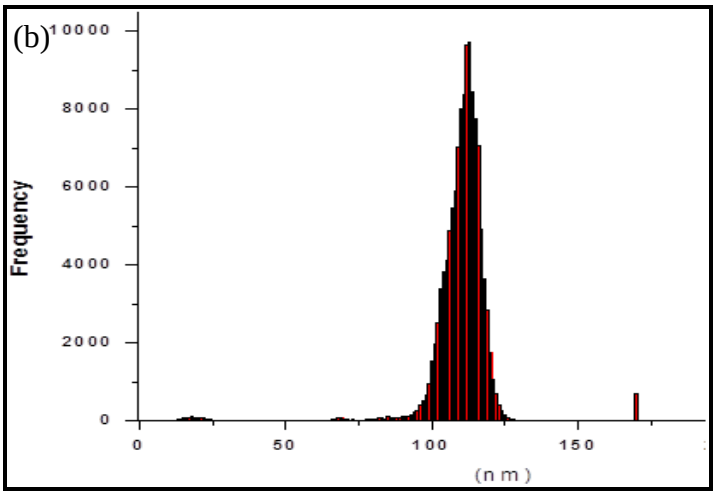


**Figure 5. 8 (a) TEM image and (b) particle size histogram of as-synthesized $Fe_3O_4$/*edta* nanoparticles.**

To understand the interaction of the *edta* ligands with the surface of $Fe_3O_4$ NPs, vibrational spectroscopy (FTIR) is one of the best tools. Figures 5.S2 and 5.S3 show the FTIR spectra of $Fe_3O_4$/*edta* and $Fe_3O_4$/*edta*/P systems respectively.

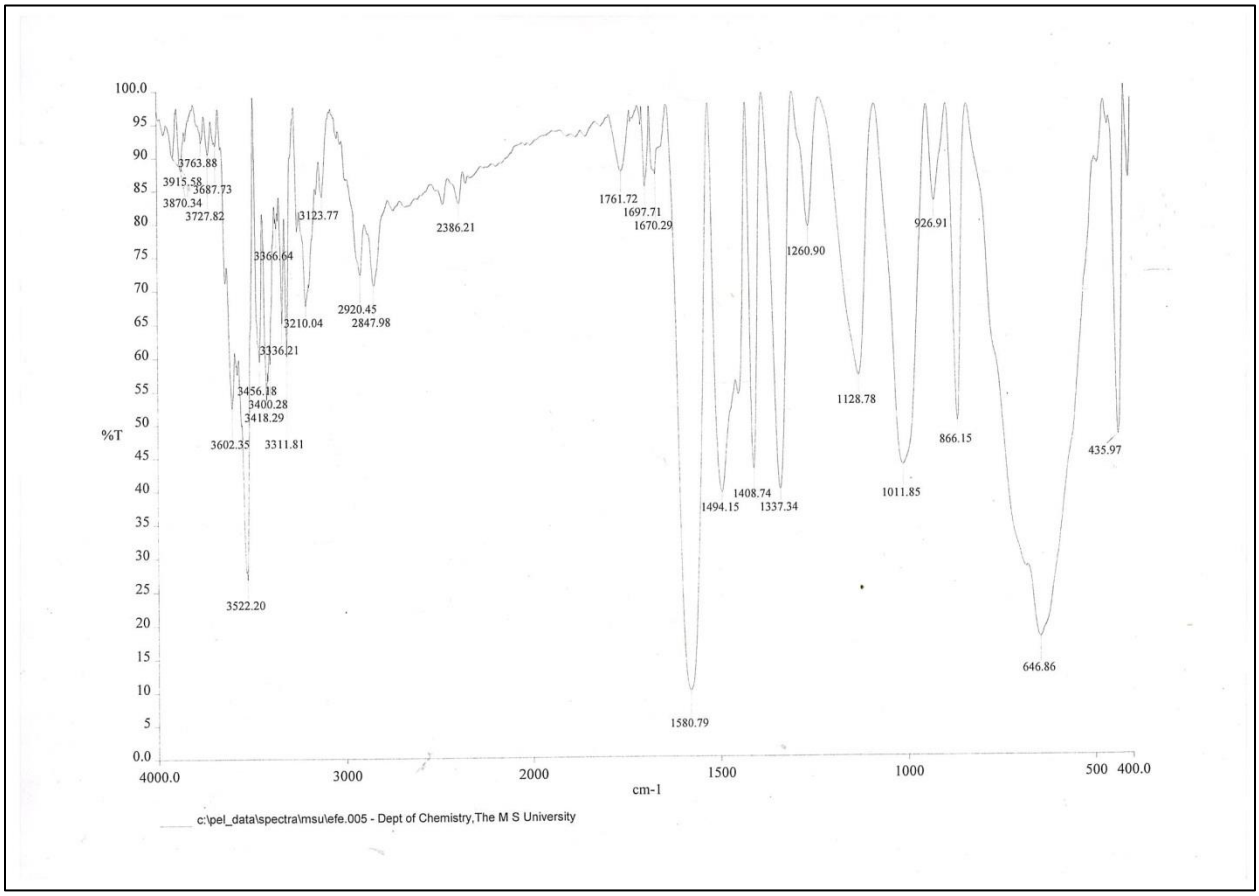


**Figure 5.S2: FTIR spectra of $Fe_3O_4$/*edta* NPs.**

.

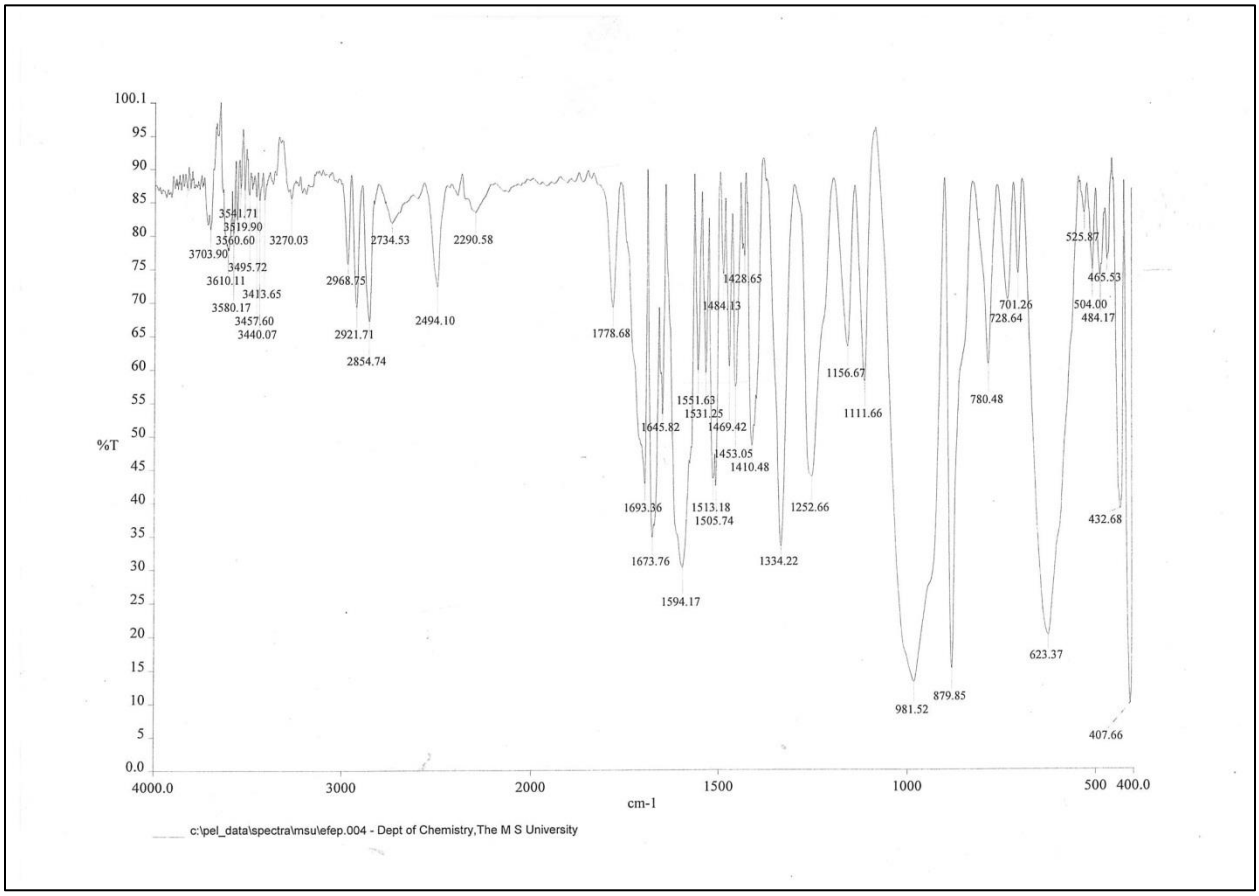


**Figure 5.S3: FTIR spectra of $Fe_3O_4$/*edta*/P magnetic micellar NPs.**

The absorption at 646 $cm^{-1}$ (Figure 5.S2) corresponds to Fe-O stretching in $Fe_3O_4$ inverse spinel system. Absorption at 1111 and 1156 $cm^{-1}$ (Figure 5.S3) are due to presence of block copolymer completely encapsulating the NPs surface and $–CH_2$-rocking of pluronic respectively. [43]*edta* possesses two nitrogen atoms and four carboxylate anions (in basic media) to coordinate with surface Fe (II/III) ions. The four carboxylate ions can coordinate with surface Fe ions either by a unidentate or a bidentate (chelating) way. [44 - 47]These can be confirmed on the basis of $COO^-$

stretching vibration frequencies. Carboxylate ions in free acetate form vibrate in two fundamental modes, asymmetric stretching $\nu_{as\ (COO^-)}$ and symmetric stretching $\nu_{s\ (COO^-)}$ at 1583 and 1422 $cm^{-1}$ respectively. [48] If carboxylate ligand coordinate with surface Fe (II/III) in a bidentate mode then, $\nu_{as\ (COO^-)}$ decreases and $\nu_{s\ (COO^-)}$ increases from the normal modes in the free state and vice versa in the case of monodentate mode. [49, 50] On comparing $\Delta\ (\nu_{as\ (COO^-)} - \nu_{s\ (COO^-)})$ with $\Delta'(\nu'_{as\ (COO^-)} - \nu'_{s\ (COO^-)})$, (where $\Delta$ is a difference in the absorption bands for free carboxylate ions and $\Delta'$ is for metal bound carboxylate ions), we found $\Delta > \Delta'$. This suggests bidentate coordination. The difference between $\nu_{as\ (COO^-)}$ (1580 $cm^{-1}$) and $\nu_{s\ (COO^-)}$ (1494 $cm^{-1}$) is below 100 $cm^{-1}$ indicating only mononuclear bidentate chelation or a combination of chelation and bridging of carboxylate ions with surface metal ions (Figure 5.3). [45]

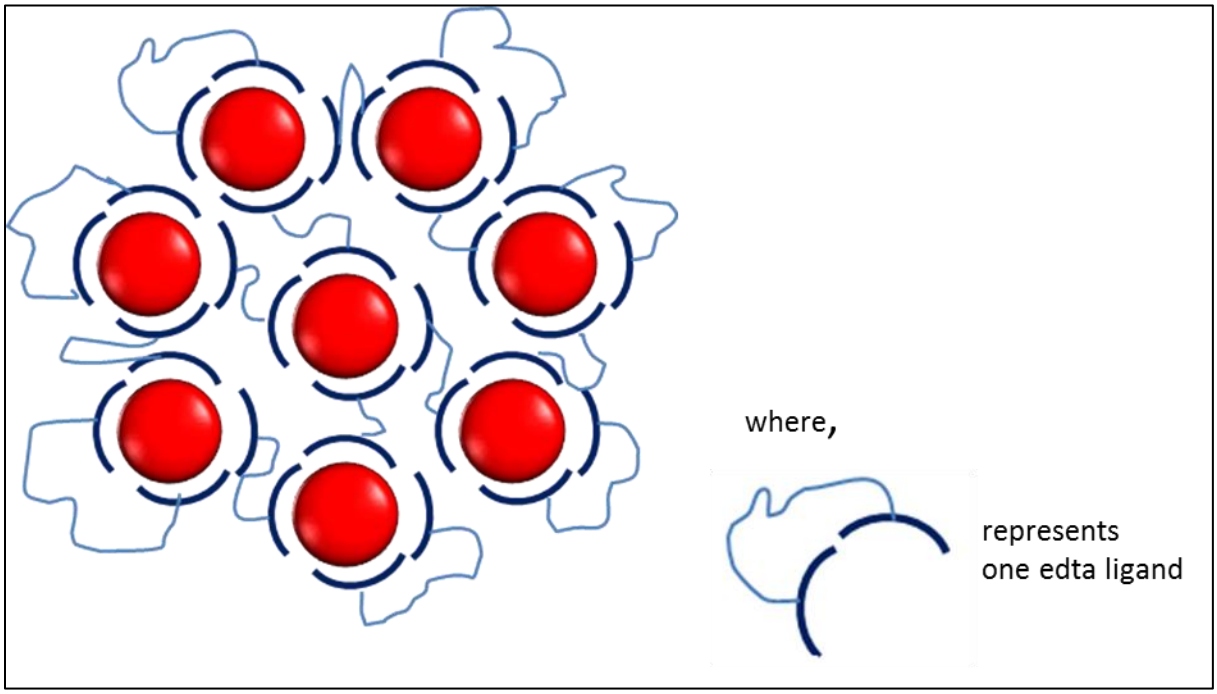


**Figure 5.9 Modes of interaction of *edta* ligands with the surface of the $Fe_3O_4$ nanoparticles- either chelating or bidentate way (red balls indicate $Fe_3O_4$ nanoparticles, one curve corresponds to two carboxylate groups and zigzag lines represent two nitrogen atoms containing hydrocarbon chains).**

The presence of pluronic layer around the surface of NPs was also confirmed by FTIR spectroscopy and TG analysis.

These micellar assemblies of NPs formed in an aqueous medium are capable of loading anti-cancer drug imatinib. Due to hydrophobic nature, imatinib should be entrapped inside the PO chains of the hydrophobic region of the pluronic shell.

### 5.3.2 Magnetic study

Magnetic properties of the synthesized $Fe_3O_4$/*edta* and $Fe_3O_4$/*edta*/P NPs were studied by VSM technique. The shape of magnetization curve (Figure 5.10) indicates superparamagnetic behavior in presence of magnetic field. It is observed that these curves do not pass directly through the origin. This is due to some residual ferromagnetic regions being present among the superparamagnetic regimes in the crystal structure of NPs. [51, 52]The magnetization and coercivity of $Fe_3O_4$/*edta* NPs were 0.4 emu/gm and 0.461G (Hci) respectively and those of drug loaded $Fe_3O_4$/*edta*/P NPs were 0.138 emu/gm and 87.61 E-3 G (Hci) respectively. The loss of magnetization may be due to the presence of hydrophobic long chains surrounding the magnetic core.

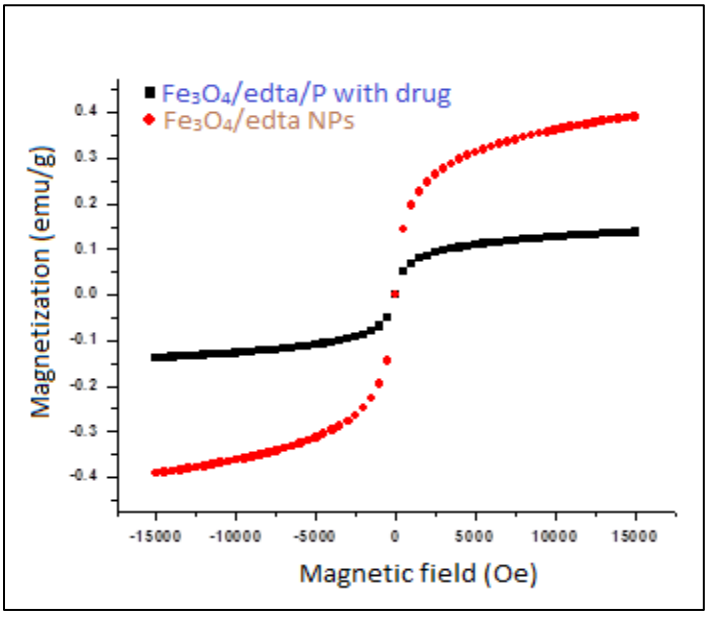


**Figure 5.10 Magnetic hysteresis loops of (a) $Fe_3O_4$/*edta* NPs (b) drug loaded $Fe_3O_4$/*edta*/P micelle.**

### 5.5.3 *In vitro* drug release kinetics, cell viability and cytotoxicity studies

The kinetics of in vitro release of imatinib from $Fe_3O_4$/*edta*/P NPs was studied in an aqueous PBS solution at pH 7.4 (Figure 5.11). It can be observed that initially ca. 30% drug was bursted within first 5 h. and it is stabilized at 48 h with overall 37.5% release. Interestingly, after this time the drug release became slow and 51.23% was released at the end of 100 h. We had extended the experiment up to 200 h. Approximately 60% drug was released at the end of 196 h. This experiment shows that the developed NPs magnetic micelle has excellent sustained drug release capacity.

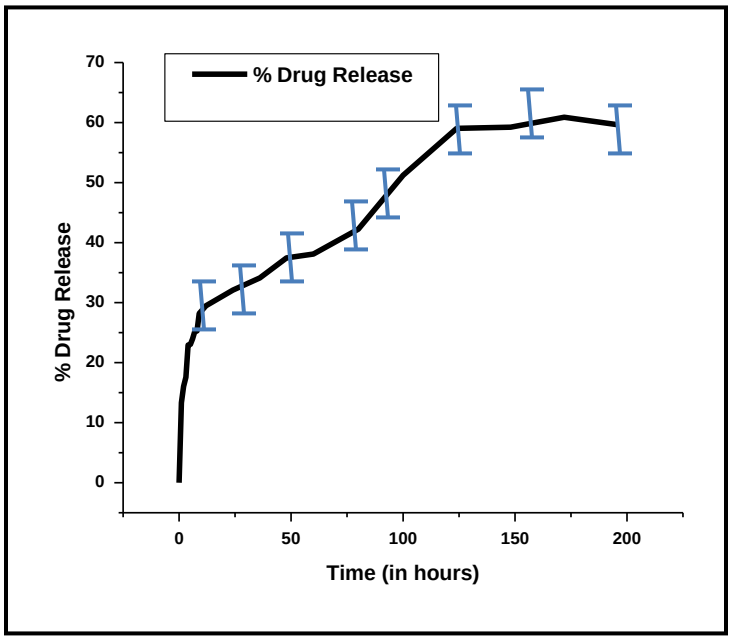


**Figure 5.11 Drug release profile of imatinib loaded $Fe_3O_4$/*edta*/P magnetic micelle.**

### 5.5.4 MTT Assay

The cytotoxic effects of different kinds of naked NPs and imatinib loaded NPs were studied by MTT assay using Chronic myeloid leukemic cell-line K562. Cell viability assay showed that no obvious cytotoxic activities were observed in K562 cells when treated with pristine $Fe_3O_4$-NPs, imatinib loaded-NPs, and bared imatinib. As shown in Figure 5.6, treatment of K562 cells with imatinib loaded-NPs caused an obvious decrease in cell viability at 48 h, as compared with that of free imatinib and $Fe_3O_4$ NPs. Over 70% cell viability is maintained in the human K562 CM leukemia cell-line after incubation for 24 and 48 h by increasing the concentration of drug loaded NPs assembly from 0.125 to 1.5 µg/mL.

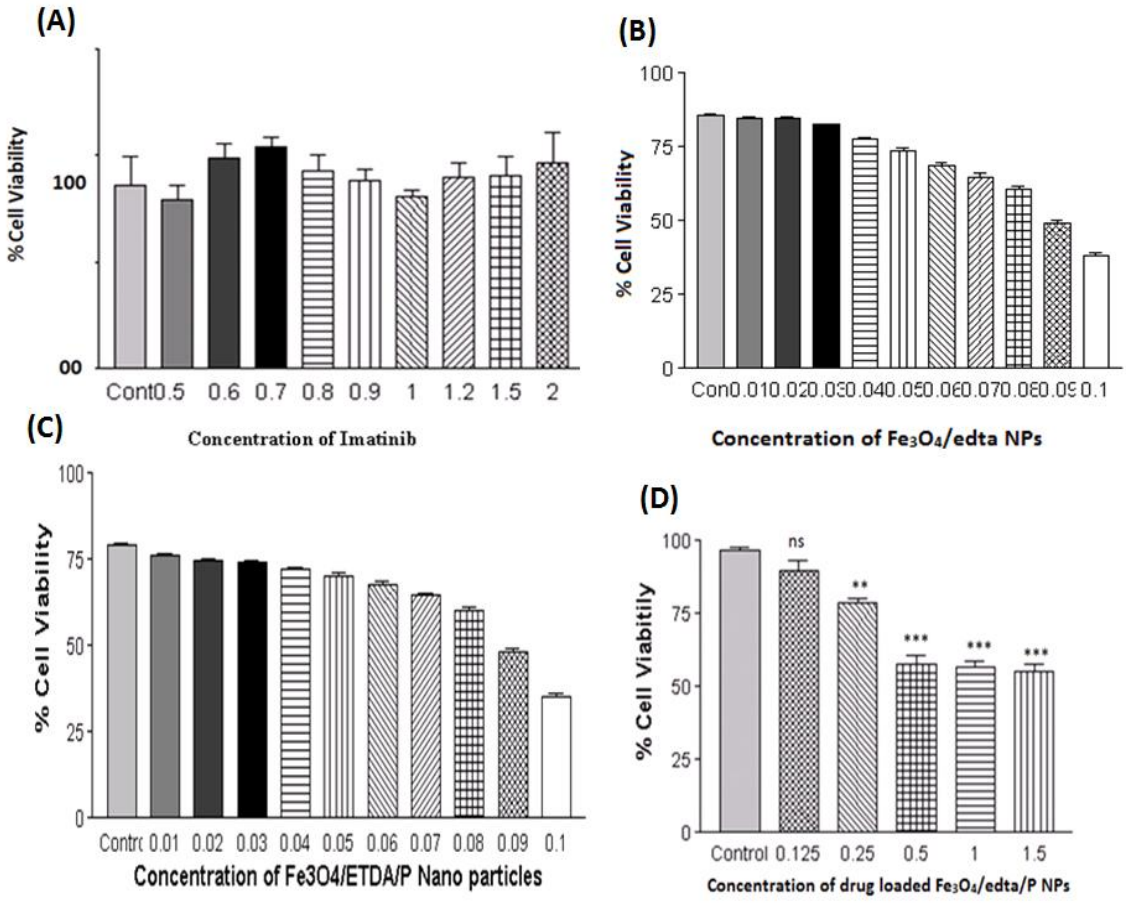


**Figure 5.12 Dose dependent effect of as synthesized NPs on cell viability of K562 cells (a) bared imatinib. Drug did not exhibit significant difference on cell viability of K562 at 0.5, 0.6, 0.7, 0.8, 0.9, 1.0, 1.2,1.5 and 2.0 µg/mL dose. p=0.6609, 0.4198, 0.2495, 0.6857, 0.8939, 0.7046, 0.8120, 0.8047 and 0.6058 respectively. (b) $Fe_3O_4$/*edta* NPs. It exhibited non-significant effect on cell viability at 0.01 and 0.02 mg/mL. p=0.0739 and 0.3040 respectively (c) $Fe_3O_4$/edta/P micelles, exhibited non-significant effect on cell viability at 0.02 and 0.03 mg/mL, p=0.0029 and 0.0022 respectively and (d) Imatinib loaded $Fe_3O_4$/*edta*/P micelles. At 0.125 drug concentration non-significant difference in the cell viability was observed (*p*=0.1621). Higher concentration (0.25, 0.5, 1, 1.5 µg/mL) significantly decreases the cell viability (*p* =0.0014, 0.0004, <0.0001 and 0.0001 respectively). The concentrations of drug as well as NPs used for this experiment did not exhibit significant difference in the cell viability under similar conditions.**

The uptake of both pristine and IM loaded $Fe_3O_4$/*edta*/P NPs micellar assembly is evaluated using the same cell line by trypan blue staining method. On repetition of the method three times, the average $IC_{50}$ value of $10^6$ cells with only drug was calculated as 0.5 µg/µL. When the experiment was carried out with drug loaded $Fe_3O_4$/*edta*/P NPs assembly, the $IC_{50}$ value of the same amount of cells was found to be 0.02 mg/mL. Hence, maximum cell viability can be achieved if the concentration of NPs assembly with drug is maintained in the range of 0.125 to 0.25 µg/mL. The TEM images (Fig.5.S4) of control and transfected cells with different amount of NPs indicate that the morphology of the cells remains same on transfection.

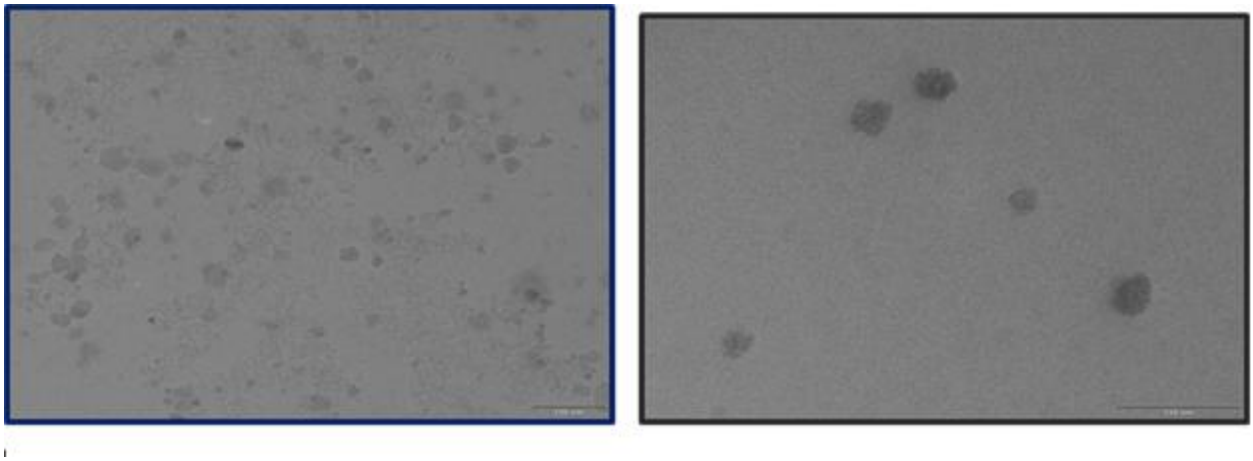

**Figure 5.S4. TEM images of (a) controlled k562 cells (b, c, and d) k562 cells transfected with $Fe_3O_4$/edta/PNPs.**

This result lead us to believe that the K562 cells adopted the apoptosis death route which is further confirmed from the microscopic images of PS-PI stained K562 cells (Figure 5.13).

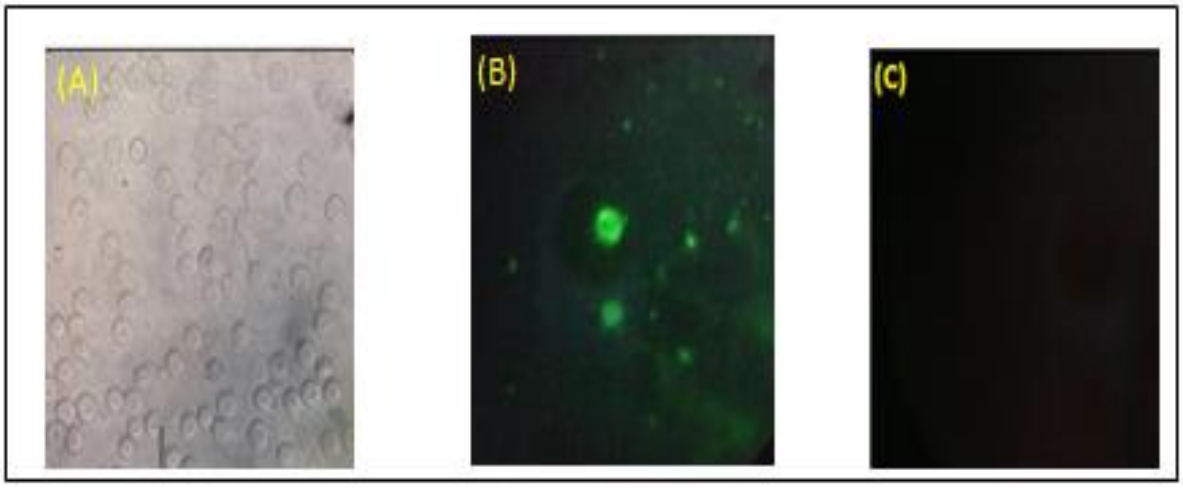


**Figure 5.13 PS-PI staining of K562 cells induced with drug . (a) Bright field image (b) PS staining (c) PI staining.**

From the cell uptake and cell viability studies it is observed that the drug loaded NPs assembly was able to transfect the cell membrane and accumulate in the cell inspite of having high hydrodynamic radius (440 nm). Particle size directly affects the accumulation kinetics of the foreign material in the cells. [53] Physiological scavenging processes that remove small foreign objects from the blood must be considered during the design of NPs based drug delivery systems. Type of capping and nature of shell (hydrophilic/hydrophobic) around the NPs core also play a role. Properly coated NPs exhibit reduced opsonization and clearance by the reticuloendothelial system. If the size of drug loaded NPs assembly larger than the glomerulus (located at the beginning of a nephron in the kidney) then renal clearance is avoided [54] and the circulating time can be extended. Furthermore,

compared to normal tissues, tumors have leaky capillaries with large fenestrations in the capillary walls that permit the passage of larger NPs system. Therefore, drug loaded into the NPs is more accessible to tumor tissues. The pore cut-off size of porous blood vessels in majority of tumors is known to be 380–780 nm and the maximum size of nanoparticles allowing penetration through cell membranes is known to be 500 nm. [55, 56] Particles having larger size (~ 500 nm) slowly diffuse in the blood vessels, however, they accumulate for longer time in the tumor cells compared to smaller ones. Hence, the drug loaded NPs assembly though larger in size than the commercially available nano-drugs or contrast agents are successful in transfecting the tumor cell lines and exhibiting the activity. [57]

### 5.5.5 *In vivo* tissue distribution

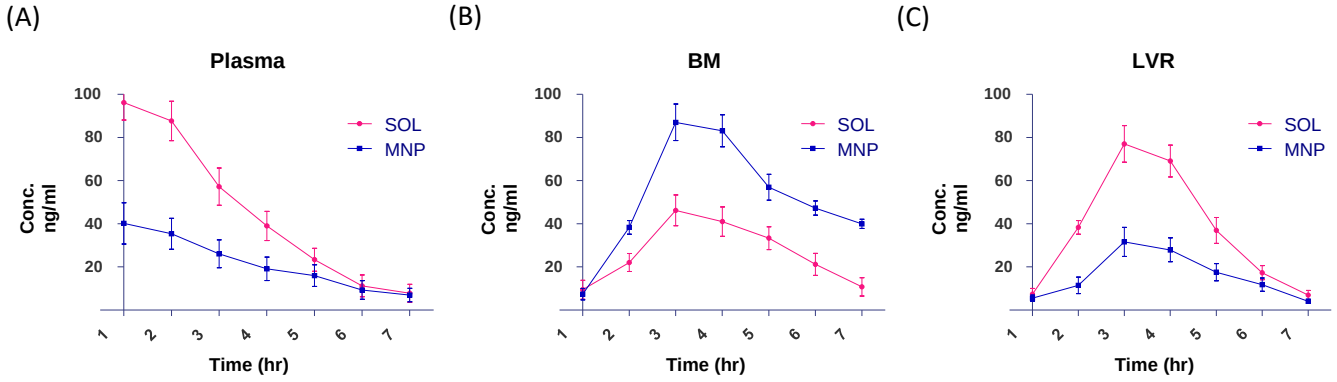


**Figure 5.14 Distribution pattern of imatinib (IM)loaded on$Fe_3O_4$/*edta*/P NPs micellar assembly in different tissues (A) blood plasma (B) bone marrow (BM) and (C) liver (LVR). SOL indicates pristine imatinib in PBS solution.**

Figure 5.14 shows distribution pattern of IM loaded on$Fe_3O_4$/edta/P NPs assembly in different tissues and the same is compared with bared (SOL) IM in PBS

solution. It can be observed that IM loaded on NPs accumulates in higher amount in BM compared to LVR and plasma. In liver, the concentration of IM loaded NPs is always lowers than the pristine IM. These results suggest that NPs formulation might minimize the hepatotoxicity of IM, by lowering the initial high concentration of IM in the liver. It can be observed that the concentration of bared IM in plasma and liver is high compared to that of IM loaded NPs. This situation results in less availability of free IM and good availability of IM loaded NPs in BM. Therefore, high dosage of drug can be delivered through synthesized micellar NPs system to BM.

### 5.5.6 Histopathological analysis

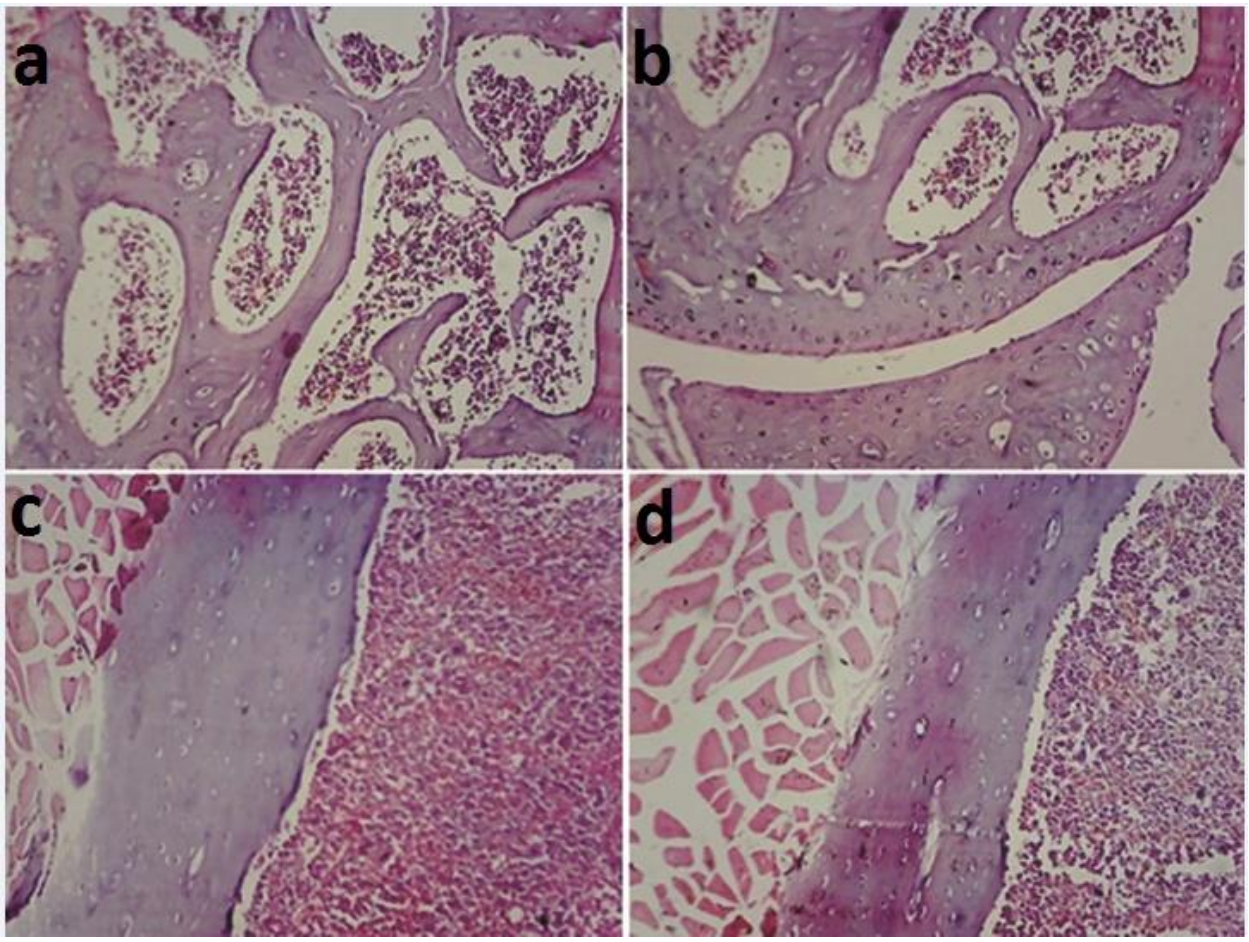


**Figure 5.15 Photomicrograph of HE stained sections of organs from the control group (a and b) and experimental groups (c and d) subjected to 100 mg $kg^{-1}$drug loaded $Fe_3O_4$/*edta*/P NPs via *i.v.* route.**

Histopathological investigation of group I mice (treated with bared IM in PBS solution) reveal moderate necrosis in BM while intensive necrosis and inflammation in liver tissues. While for that of group II mice (treated with IM loaded NPs) no major histochemical alteration was observed in BM with no evidence of necrosis (Figure 5.15). This indicates that pristine imatinib exerts

petite toxic effect on these tissues at defined dose through *i.v.* administration. No evidence of toxicity in marrow signifies that IM with NPs formulation is safe when administered through *i.v.* route.

### 5.5.7Phantom Study

In the present work, $Fe_3O_4$/*edta*/P assembly can work as $T_1$-$T_2$ dual contrast agent in aqueous media. The correlation between $T_1$, $T_2$ relaxation rates ($R_1$ and $R_2$) and the concentration of synthesized NPs was investigated in a phantom experiment. Visible signal decay (i.e. darker images w.r.t background) in both $T_1$ and $T_2$-weighted images with increased concentration of synthesized NPs can be clearly observed (Figure 5.16). It is observed from Fig. 5.16 that contrasting effect can be achieved at concentration of NPs as low as 0.001 M. This is preferred for clinical use of the material as a contrast agent to generate appropriate signal with minimal level of associated risk.

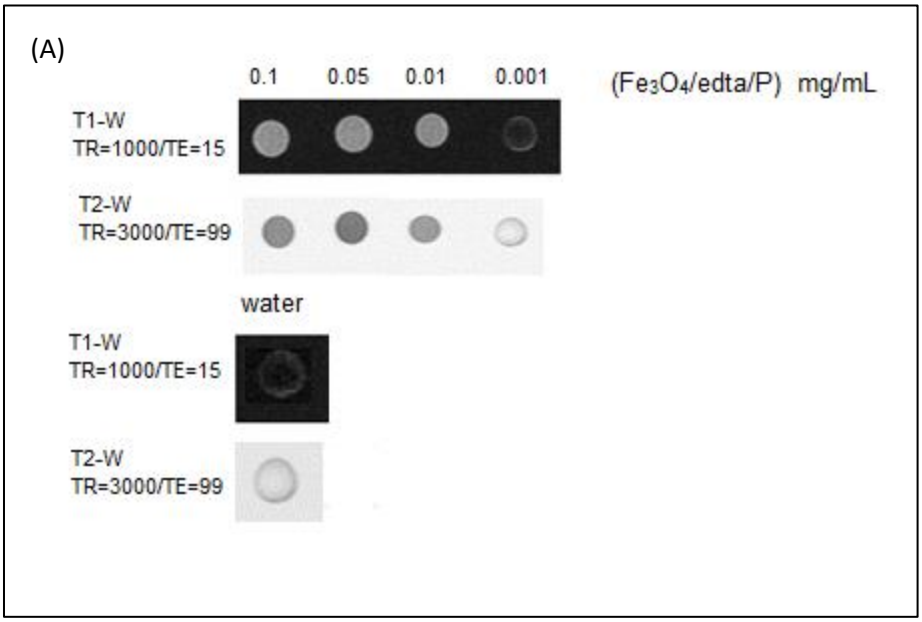


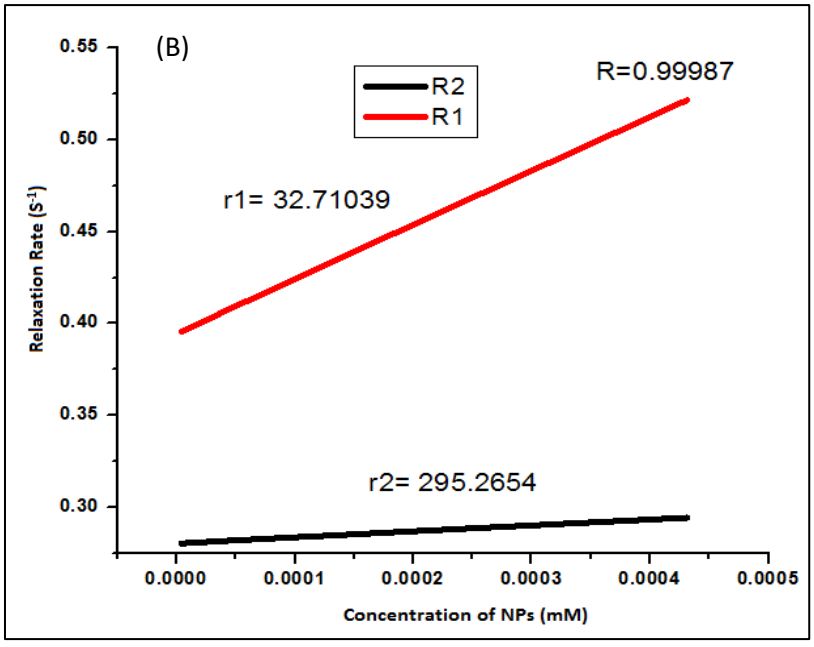


**Figure 5.16 (A) $T_2$-weighted (TR=3000/TE=99ms) and $T_1$ weighted (TR=1000/TE=15ms) MR images at different concentrations of $Fe_3O_4$/*edta*/P NPs and the same are compared with water as background (B) Correlation between $R_1$, $R_2$ and concentration of $Fe_3O_4$/*edta*/P NPs.**

The efficiency of MRI contrast agent is evaluated in terms of longitudinal ($T_1$) and transverse ($T_2$) relaxation times. Gd based chelates shorten the $T_1$ while magnetic NPs shorten $T_2$.[58] Figure 5.10 (b) shows dependence of proton relaxation rate ($1/T_1$ or $1/T_2$) on the concentration of synthesized NPs magnetic micelles. It can be observed that relaxation rate varies linearly with concentration of NPs. The longitudinal relaxivity ($r_1$) and transverse relaxivity ($r_2$) calculated from the slope of the curves are 32.71 and 295.27 $mM^{-1}s^{-1}$, respectively.

The $r_1$ and $r_2$ values of clinically used and commercially available contrast agents are compared with synthesized NPs in Table 5.1. From Table 5.1, it can be concluded that the synthesized $Fe_3O_4$/*edta*/P micellar system can act as $T_1$-$T_2$ dual mode contrast agent.

**5.5.8 *In vivo* animal imaging**. For further validation, these nanoparticles assembly were injected intravenously in rat. Figure 5.14 shows the bone marrow of mice at different stages. The $T_1$ and $T_2$ weighted images acquired 15 min after the injection clearly differentiates the bone marrow from the remaining part of the body generating both brighter and darker contrast. The contrasting effect became more significant after 24 h. Further anatomical information could not be extracted due to the lower magnetic field (1.5 T) of the MRI instrument used and also, we were not able to induce the tumor (possibly due to type of cancer selected for the study) and

map the same to show the efficacy of drug loaded synthesized NPs, through MRI. However, we could establish the utility of as-synthesized NPs as $T_1$-$T_2$ dual mode contrast agents.

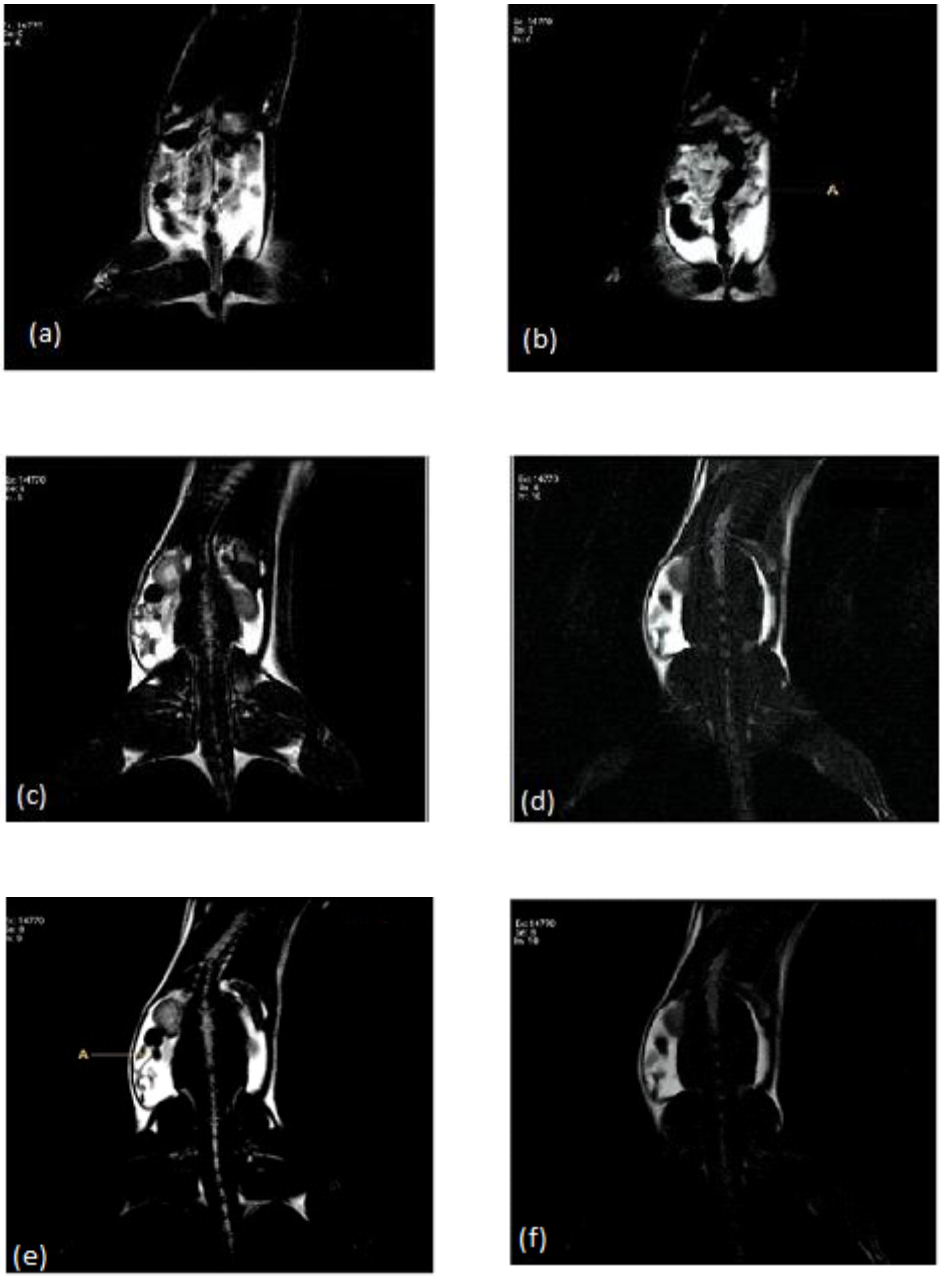


**Fig. 5.17 MR images of synthesized $Fe_3O_4$/*edta*/P NPs injected mouse (a, b) $T_1$-weighted and**

**$T_2$-weighted images prior to injection of NPs, (c, d) $T_1$-weighted and $T_2$-weighted images 15 min post injection of NPs, (e, f) $T_1$-weighted and $T_2$-weighted images 24 h post injection of NPs.**

To establish the mechanism of $T_1$-$T_2$ dual contrasting effect revealed by the synthesized magnetic micelles we had carried out zeta potential measurements and TGA analysis. From surface charge measurements it can be observed that pristine $Fe_3O_4$/*edta* NPs possess negatively charged surface with a ζ value -23.87 mV and, on addition of pluronic it decreases to -1.73 mV. Emergence of charge on the surface is directly influenced by the presence of counter ions in the medium and the mode of crystallization. Obviously, the negative charge on the surface of $Fe_3O_4$/*edta* is due to presence of $^{-}$OH ions in the basic aqueous medium. During the crystal growth, $^{-}$OH ions as well as *edta* both act as capping ligands, however,

$^{-}$OH ions are more prone to be adsorbed on the surface due to charge while *edta* makes coordination bond with the surface Fe (II/III) ions. On pluronic encapsulation, the rising hydrophobicity expels some $^{-}$OH ions with some polar water molecules from the surface. However, the polar molecules could not be totally expelled due to H-bonding with N atoms of surface coordinated *edta*. The decrease in ζ value to -1.73 mV corroborates the expulsion of $^{-}$OH ions from the surface. We had carried out TGA studies of the $Fe_3O_4$/*edta*/P NPs for further confirmation. Two major weight losses, at 85 and 112 $^{o}$C, occur due to bulk water

and surface bounded water respectively (Figure 5.18). The weight loss at 316 $^{o}$C is due to carbonization of the *edta* ligand.

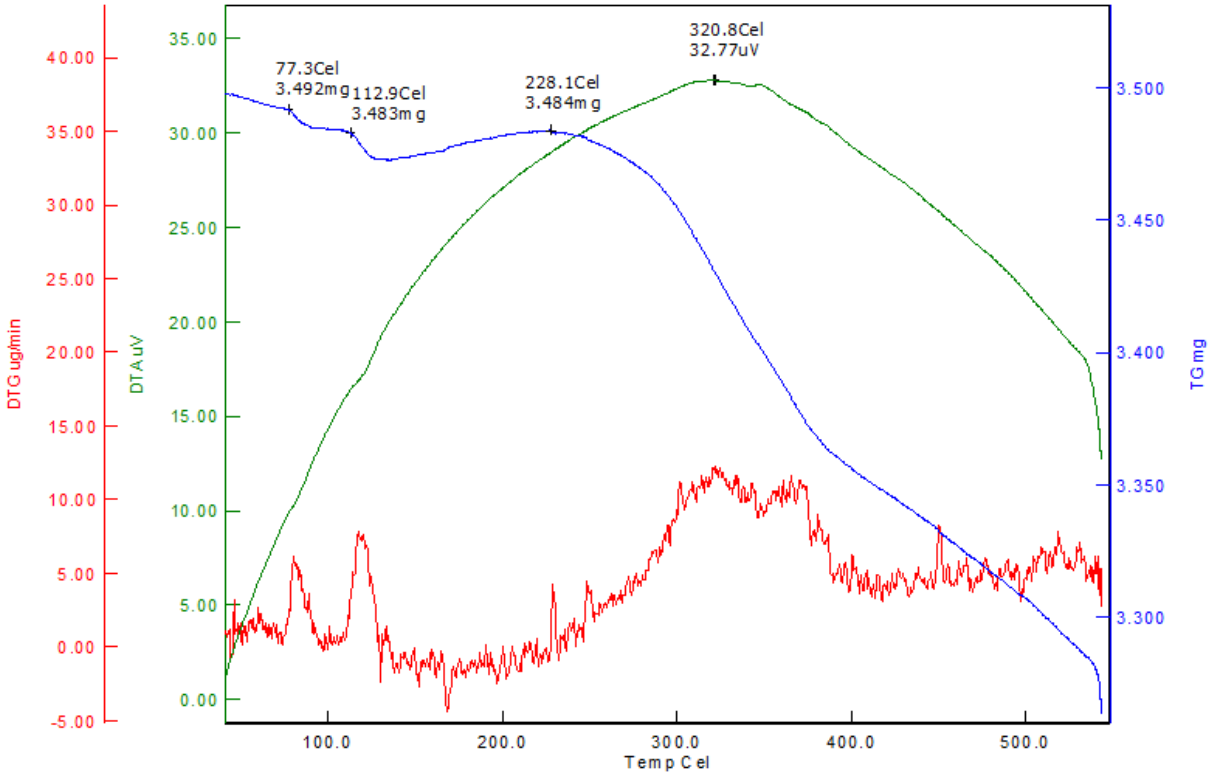


**Figure 5.18 Thermal analysis of $Fe_3O_4$/*edta*/P magnetic micellar system.**

From these studies, it is clear that magnetic micelle of $Fe_3O_4$/*edta*/P NPs are formed under the experimental conditions in aqueous medium in which hydrophilic EO chains containing blocks of pluronic form core and hydrophobic PO blocks form shell and the nitrogen atoms of edta provide sites for H-bonding for polar molecules like water and $^{-}$OH ions (Figure 5.13).

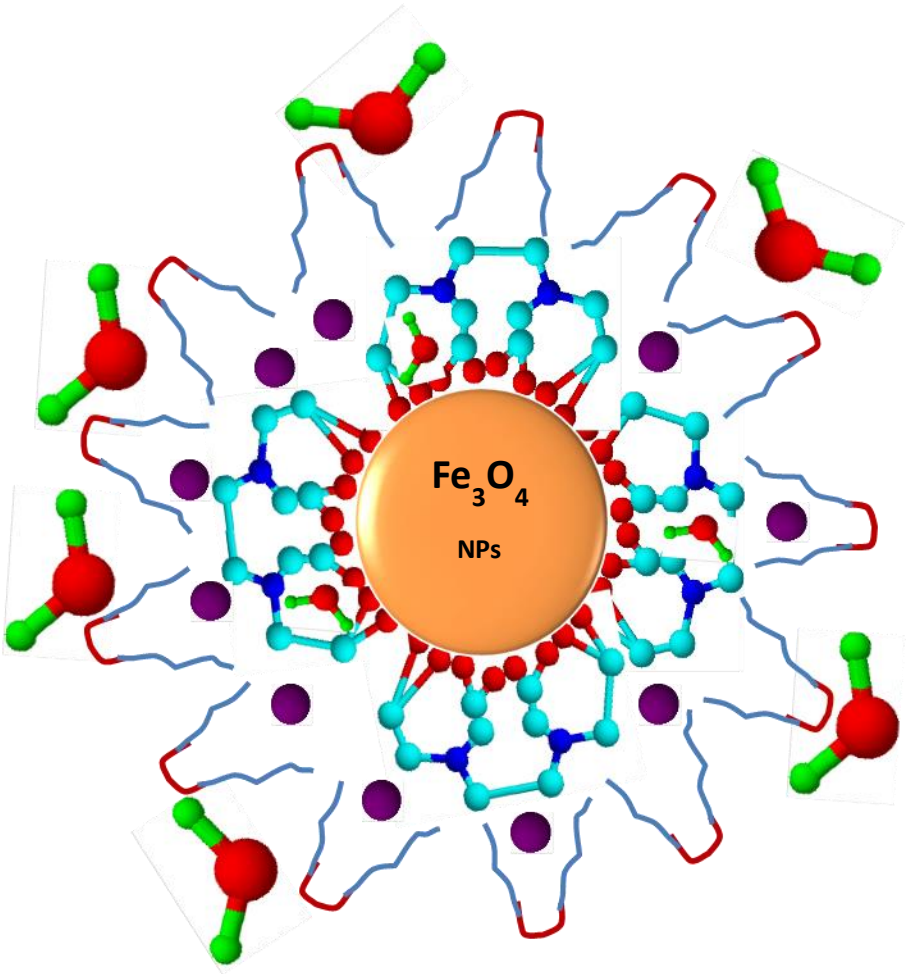


**Figure 5.19 Cartoon showing $Fe_3O_4$/*edta*/P magnetic polymeric micelle. Central orange ball representing $Fe_3O_4$ nanoparticle surrounded by edta ligands (blue balls indicates nitrogen, light blue for carbon, red for carboxylate group, purple for drug molecule). The zigzag light blue lines correspond to hydrophobic PPO blocks while that of red to hydrophilic PEO blocks. Some water molecules can be seen entrapped near the ligand's nitrogen atoms by coordination bond while the polymeric micelle is surrounded by second sphere water molecules.**

From this structure, we propose that $r_2$ relaxivity is achieved due to particle size and super paramagnetic property of $Fe_3O_4$ NPs. The manifestation of $r_1$ relaxivity is due to protons of two types of water molecules, one bounded with *edta* ligand through H-bonding near the surface on NPs and the other are the bulk water molecules of the aqueous medium present at hydrophilic/hydrophobic interface of magnetic micelle. This situation is the mimic of Gd-DTPA chelate chemistry-known for $r_1$relaxivity. These results encourage further research in the field to induce $T_1$-$T_2$ dual modalities in a sole material.

**Table 5.1. Hydrodynamic diameter or particle size and different relaxivity parameters of various systems reported in the literature.**

| Sample Name | Surface Coating | Mean hydrody-namic diameter (or Core size) (nm) | Longitudinal Relaxivity[a] $r_1$ ($s^{-1}mM^{-1}$) | Transverse Relaxivty[a] $r_2$ ($s^{-1}mM^{-1}$) | Reference |
|---|---|---|---|---|---|
| Oleate capped CoO NCs functionalized with CTAB. COA@CoO | CTAB/OA | 302 | 0.2 | 2.0 | 59 |
| Oleate capped CoO NCs functionalized with SDS. SOA@CoO | SDS/OA | 316 | 0.4 | 4.0 | 59 |
| Oleate capped CoO NCs functionalized with CTAB. | PF127/OA | 231 | 1.2 | 31.2 | 59 |

| | | | | | |
|---|---|---|---|---|---|
| POA@CoO | | | | | |
| Lanthanum Strontium Manganese Oxide NPs. (LSMO NPs) | Dextran | ≤ 50 | 6.741 ($s^{-1}mg^{-1}mL$) | 778 ($s^{-1}mg^{-1}mL$) | 58 |
| SPION | Folate-bovine serum albumin (FA-BSA) | 196.1 | - | 179.5 | 57 |
| SPION | Copolymer o poly (ethylene glycol) and poly(ε-caprolactum) bearing folate. (Fa-PEG-PCL) | 125.2 ± 2.3 | 2.1 | 121.2 | 60 |
| SPION | Poly (succinimide) grafted with folate conjugated poly (ethylene glycol) and alkyl chains. | 38.1±10.4 | - | 227 | 61 |
| Gold nano shells | Silica epilayer doped with $Fe_3O_4$ and functional ized with fluorophore - indocyanine | 74 | - | 390 | 62 |

| | | | | | |
|---|---|---|---|---|---|
| | (ICG) | | | | |
| Polystyrene | Functionalized with mixed-metal oxo cluster $Mn_8Fe_4O_{12}(L)_{16}(H_2O)_4$. Where L = acetate or vinyl benzoic acid. | Bead diameter 100 nm | 2.3 | 29.5 | 63 |
| $ZnFe_2O_4$ NPs | Chitosan nanospheres | 6.65±1.1 | - | 239 | 64 |
| $Fe_3O_4$/*edta* | Pluronic-F127 | 232 | 32.71 | 295.26 | *(This study)* |
| Gd-DTPA-Dopamine-BisphytanylAmphiphiles | Pluronic-F108 | - | 14.2 | 15.8 | 65 |
| Resovist® | Carboxy dextran | 65 | 25 | 164 | 66 |
| Feridex® | Dextran | 72 | 40 | 160 | 67 |

[a]The $r_1$ and $r_2$ values reported here for commercial contrast agents may be varied with the literature values depending on the magnetic field strength used for the experiment, MR pulse sequences, particle size, coating material etc.

## 5.6Conclusion

Small molecules like *edta* can act as capping and chelating ligand to bind $Fe_3O_4$ nanoparticles tightly and restrict the growth at nano regime. Pluronic F127 encapsulates these *edta* capped $Fe_3O_4$ nanoparticles and form micelle with retaining superparamagnetic property. The synthesized pluronic encapsulated and *edta* capped $Fe_3O_4$ magnetic micelle can be loaded with hydrophobic anti-cancer drug like imatinib in their hydrophobic shells. In vitro cellular uptake study with human bone marrow K562 cell-line shows these drug loaded magnetic micelles are internalized to a higher extent than the bared drug. The overall size of the drug loaded magnetic micelles allowed prolong circulation and sustained drug delivery. Elaborate toxicity studies confirm the safety of the developed iron oxide nanoparticle based magnetic micelles as drug delivery vehicle to a dosage in the range of 0.125-0.25µg/mL after intravenous administration. In vivo study of distribution pattern of imatinib in various tissues (like liver, bone marrow and blood plasma) shows that high dosage of drug can be delivered to bone marrow using synthesized micellar nanoparticles as vehicle. If synthesis is carried out in aqueous medium then some water molecules can be entrapped either by coordination with the surface ions or by H-bonding with the ligand used to restrict the growth of the nanoparticles. These coordinated water molecules can mimic the Gd based $T_1$ (bright) magnetic resonance imaging contrast agent. The super paramagnetic nanoparticles themselves act as $T_2$ (dark) contrast agent. Hence, both

$T_1$ and $T_2$ contrasting abilities can be achieved in a sole material. This work can provide a direction to the future research for designing Gd free $T_1$-$T_2$ dual mode contrasting agents.

## References


1 A. Jemal, F. Bray, M. M. Center, J.Ferlay, E. Ward and D. Forman, *Cancer J Clin*., 2011, **69**, 61.

2 R. Siegel, D. Naishadham and A. Jemal, *Cancer J Clin*., 2013, **11**, 63.

3 N. Milosavljevic, C. Duranton, N. Djerbi, P. H. Puech, P. Gounon, D.Lagadic-Gossmann, M. T. Dimanche-Boitrel, C. Rauch, M. Tauc, L. Counillon and M. Poët, *Cancer Res.*, 2010**, 7514**,70.

4 M. C. Perry, In *The Chemotherapy Source Book*, 5th edition, Lippincott Williams and Wilkins, 2012.

5 G. Tiwari, R. Tiwari and A. K. Rai, *J. Pharm. Bioallied Sci.*, 2010, **72**, 2.

6 J. Zhang and P. X. Ma, *Adv. Drug Deliver. Rev.*, 2013, **1215**, 65.

7 U. Kedar, P. Phutane, S. Shidhaye and V. Kadam, *Nanomedicine: Nanotechnology, Biology and Medicine,* 2010, **714**, 6.

8 G. S. Kwona and T. Okano, *Adv. Drug Deliver. Rev.*,1996, **107**,21.

9 A. M. Mintzer and E. E.Simanek, *Chem. Rev.*,2009, **259**,109.

10 P. Tanner, P. Baumann, R.Enea, O. Onaca, C. Palivan and W. Meier, *Acc. Chem. Res.*,2011, **1039**,44.

11 T.-H.Shin, Y. Choi, S. Kim and J. Cheon, *Chem. Soc. Rev.*,2015, **4501**,44.

12 D. Ho, X. Sun and S. Sun, *Acc. Chem. Res.*,2011, **875**,44.

13 A. K. Gupta and M. Gupta, *Biomaterials,*2005, **3995**, 26.

14 J. Chomoucka, J. Drbohlavova, D.Huska, V. Adam, R. Kizek and J.Hubalek, *Pharmacol. Res.*, 2010, **144,** 62.

15 B. D. Cullity, In Introduction to magnetic materials. Addision Wesley Pub. Company, Reading, MA, 1972.

16 Q. A. Pankhurst, J. Connolly, S. K. Jones and J. Dobson, *J. Phys. D: Appl. Phys*., 2003, **R161**, 36.

17 Y. –W.Jun, Y. –M.Huh, J. –S.Choi, J. –H.Lee, H. –T.Song, S. Kim, S. Yoon, K. –S.Kim, J. –S.Shin, J. –S.Suh and J. Cheon, *J. Am. Chem. Soc.*,2005, **5732,** 127.

18 H. –M.Liu, J. –K. Hsiao,In Smart nanoparticle technology. (Ed.: A. Hashim), InTech Publication, 2012**,** Ch.16.

19 S. Warner, *Scientist,* 2004, **38**, 18.

20 Y. X.Wang, S. M. Hussain, G. P. Krestin, *Eur. Radiol*., 2001, **2319**, 11.

21 A. Merbach, L. Helm and E. Toth, In The Chemistry of Contrast Agents in Medical Magnetic Resonance Imaging. John Wiley & Sons Ltd, Chichester, UK, 2013.

22 R. E. Lauffer,*Chem. Re*v.,1987, **901**, 87.

23 H. B. Na, I. C. Song and T.Hyeon, *Adv. Mater*.,2009, **2133**, 21.

24 P. Verwilst, S. Park, B. Yoon and J. S. Kim,*Chem. Soc. Rev*., 2015, **1791**, 44.

25 J. W. M. Bulte and D. L. Kraitchman, *NMR Biomed*.,2004, **484**, 17.

26 K. H. Bae, Y. B. Kim, Y. Lee, J. H. Wang, H. Park and T.G. Park,*Bioconjugate Chem.*,2010, **505**, 21.

27 Z. Zhou, D. Huang, J.Bao, Q. Chen, G. Liu, Z. Chen, X. Chen, X and J. A. Gao,*Adv. Mater.*,2012, **6223**, 24.

28 G. Huang, H. Li, J. Chen, Z. Zhao, L. Yang, X. Chi, Z. Chen, X. Wang and J.Gao,*Nanoscale*,2014, **10404**, 6.

29 S. E. Cowper, L.D. Su, J.Bhawan, H. S. Robin and P. E. LeBoit,*Am. J.Dermatopathol.*,2001, **383**, 23.

30 T. Grobner,*Nephrol. Dial. Transplant.*,2006, **1104**, 21.

31 D. J. Todd, A.Kagan, L. B. Chibnik and J. Kay,*Arthritis Rheum.*,2007, **3433**, 56.

32 S. G. O'Brien, F. Guilhot and R. A. Larson, *N. Engl. J. Med*.,2003, **994**, 348.

33 S. Hodgson,*J. Zhejiang Univ. Sci. B*,2008, **1**, 9.

34 A. Arora and E. M. Scholar,*J.Pharmacol. Exp. Ther.*,2005, **971**, 315.

35 V. Malhotra and M. C. Perry,*Cancer Biol. Ther*.,2003, **S2**, 2.

36 G. Makin and J. A. Hickman,*Cell Tissue Res.*,2000, **143**, 301.

37 M. Breccia and G. Alimena,*Cancer Lett.*,2012, **18**, 325.

38 B. Stein and B. D. Smith,*Clin. Ther.*,2010, **804**, 32.

39 I. C. Macdougall, *Kidney Int. Suppl*., 1999, **S61**, 69.

40 E. Shah, P.Mahapatra, A. V. Bedekar and H. P. Soni, *RSC Adv.*,2015, **26291**, 5.

41 S. Kerkhofs, T. Willhammar, H. V. D. Noortgate, C. E. A.Kirschhock, E. Breynaert, G. V. Tendeloo, S. Bals and J. A. Martens, *Chem. Mater*.,2015, **5161**, 27.

42 R. Jenkins and R. L. Snyder, Introduction to X-ray Powder Diffractometry. John Wiley & Sons, NY, 1996.

43 T. K. Jain, M. A. Morales, S. K.Sahoo, D. L. Leslie-Pelecky and V.Labhasetwar, *Mol. Pharm.*,2005, **194**, 2.

44 P. S. Subramanian, P. C. Dave, V. P. Boricha and D. Srinivas,*Polyhedron*,1998, **443**, 17.

45 G. B. Deacon and R. Philips,*J. Coord. Chem. Rev.*,1980, **227**, 33.

46 F. P. Tania, L. Werner, P. W. Smet, G. G. Herman and A. M. Goeminne,*Polyhedron*,1999, **1029**,18.

47 E. Shah and H. P. Soni, *RSC Adv.*, 2013, **17453**, 3.

48 A. Barth,*Prog. Biophys. Mol. Biol.*,2000, **141**, 74.

49 M. Kakihana, T.Nagumo, M. Okamoto and H. Kakihana,*J. Phys. Chem.*,1987, **6128**, 91.

50 P. R. Desai, N. J. Jain, R. K. Sharma and P. Bahadur, *Colloid Surf. A*, 2001, **57,** 178.

51 J. Chomoucka, J. Drbohlavova, D.Huska, V. Adam, R. Kizek and J.Hubalek, *Pharmacol. Res.*, 2010, **144**, 62.

52 L. Li, Y. Yang, J. Ding and J. M. Xue, *Chem. Mater*.,2010, **3183**,22.

53 K. F. Pirollo and E. H. Chang, *Trends Biotechnol.*, 2008**, 552**, 26.

54 R. A. Siegel and M. J. Rathbone, in J. Siepmann et al. (eds.), Fundamentals and Applications of Controlled Release Drug Delivery, Advances in Delivery Science and Technology, Controlled Release Society, ch.2, 2012, DOI 10.1007/978-1-4614-0881-9_2.

55 S. K. Hobbs, W. L. Monsky, L. Yuan, W. G. Roberts, L. Griffith, V. P.Torchilin and R. K. Jain, *Proc. Natl. Acad. Sci*., 1998**, 4607**, 95.

56 Y. H. Bae and K. Park, *J. Control.Release*., 2011, **198**, 153.

57 H. Li, K. Yan, Y. Shang, L.Shrestha, R. Liao, F. Liu, P. Li, H. Xu, Z. Xu and P. K. Chu,*ActaBiomater*.,2015, **117**, 15.

58 R. Haghniaz, K. R. Bhayani, R. D. Umrani and K. M.Paknikar,*RSC Adv*.,2013, **18489**, 3.

59 H. Yang, H. Zhou, C. Zhang, X. Li, H. Hu, H. Wu and S. Yang, *Dalton Trans*., 2011, **3616**, 40.

60 D. Cheng, G. Hong, W. Wang, R. Yuan, H. Ai, J.Shen, B. Liang, J. Gao and X. Shuai, *J. Mater. Chem.*, 2011, **4796**, 21.

61 H. –M. Yang,C. W. Park, P. K.Bae, T.Ahn,B. –K.Seo, B. H. Chung and J. –D. Kim, *J. Mater. Chem. B*, 2013, **3035**, 1.

62 R. Bardhan, W. Chen, C. Perez-Torres, M. Bartels, R. M. Huschka, L. L. Zhao, E. Morosan, R. G. Pautler, A. Joshi and N. J. Halas,*Adv. Funct. Mater.*, 2009, **3901**, 19.

63 M. H. Pablico-Lansigan, W. J. Hickling, E. A.Japp, O. C. Rodriguez, A.Ghosh, C. Albanese, M. Nishida, E. V. Keuren, S. Fricke, N. Dollahon and S. L. Stoll,*ACS Nano*, 2013, **9040**, 7.

64 Y. Lin, W. Yao, Y. Cheng, H.Qian, X. Wang, Y. Ding, W. Wu and X. Jiang, *J. Mater. Chem.*,2012, **5684**, 22.

65 A. Gupta, S. A. Willis, L. J. Waddington, T. Stait-Gardner, L. de Campo, D. W. Hwang, N. Kirby, W. S. Price and M. J. Moghaddam, *Chem. Eur. J.*,2015, , **13950**, 21.

66 T. Allkemper, C. Bremer, L. Matuszewski, W. Ebert and P. Reimer, *Radiology*, 2002, **432**, 223.

67.L. Josephson, J. Lewis, P. Jacobs, P. F. Hahn and D. D. Stark, *Magn. Reson. Imaging*, 1988, **647**, 6.